JGR Oceans

RESEARCH ARTICLE
10.1029/2021JC017563

Key Points:

- We present a novel approach to utilizing naturally felled driftwood as a proxy for Arctic Ocean surface circulation and sea ice dynamics
- A 500-year record of driftwood incursion to Svalbard reflects centennial to decadal variability in surface circulation and sea ice extent
- A distinct decrease in driftwood from all provenances in the last 30 years matches the observed decline in pan-Arctic sea ice extent

Supporting Information:

Supporting Information may be found in the online version of this article.

Correspondence to:

G. M. Hole,
georgia.hole@ouce.ox.ac.uk

Citation:

Hole, G. M., Rawson, T., Farnsworth, W. R., Schomacker, A., Ingólfsson, Ó., & Macias-Fauria, M. (2021). A driftwood-based record of Arctic sea ice during the last 500 years from northern Svalbard reveals sea ice dynamics in the Arctic Ocean and Arctic peripheral seas. *Journal of Geophysical Research: Oceans*, *126*, e2021JC017563. https://doi.org/10.1029/2021JC017563

Received 14 MAY 2021
Accepted 30 AUG 2021

Author Contributions:

Conceptualization: Georgia M. Hole, Marc Macias-Fauria
Data curation: Georgia M. Hole
Formal analysis: Georgia M. Hole, Thomas Rawson
Funding acquisition: Georgia M. Hole, Marc Macias-Fauria
Investigation: Georgia M. Hole, Wesley R. Farnsworth, Anders Schomacker, Marc Macias-Fauria
Methodology: Georgia M. Hole, Marc Macias-Fauria

A Driftwood-Based Record of Arctic Sea Ice During the Last 500 Years From Northern Svalbard Reveals Sea Ice Dynamics in the Arctic Ocean and Arctic Peripheral Seas

Georgia M. Hole[1], Thomas Rawson[2], Wesley R. Farnsworth[3,4], Anders Schomacker[5], Ólafur Ingólfsson[4,6], and Marc Macias-Fauria[1]

[1]Biogeosciences Research Group, School of Geography and the Environment, University of Oxford, Oxford, UK, [2]Department of Zoology, Mathematical Ecology Research Group, University of Oxford, Oxford, UK, [3]Nordic Volcanological Center, University of Iceland, Reykjavík, Iceland, [4]Department of Arctic Geology, The University Centre in Svalbard (UNIS), Longyearbyen, Norway, [5]Department of Geosciences, UiT The Arctic University of Norway, Tromsø, Norway, [6]Faculty of Earth Sciences, University of Iceland, Reykjavík, Iceland

Abstract We present a 500-year history of naturally felled driftwood incursion to northern Svalbard, directly reflecting regional sea ice conditions and Arctic Ocean circulation. Provenance and age determinations by dendrochronology and wood anatomy provide insights into Arctic Ocean currents and climatic conditions at a fine spatial resolution, as crossdating with reference chronologies from the circum-Arctic boreal forests enables determination of the watershed the driftwood originated from. Sample crossdating may result in a wide range of matches across the pan-boreal region, which may be biased toward regions covered by the reference chronologies. Our study considers alternate approaches to selecting probable origin sites, by weighting scores via reference chronology span and visualizing results through spatiotemporal density plots, as opposed to more basic ranking systems. As our samples come from naturally felled trees (not logged or both), the relative proportions of different provenances are used to infer past ocean current dominance. Our record indicates centennial-to decadal-scale shifts in source regions for driftwood incursion to Svalbard, aligning with Late Holocene high variability and high frequency shifts in the Transpolar Drift and Beaufort Gyre strengths and associated fluctuating climate conditions. Driftwood occurrence and provenance also track the northward ice formation shift in peripheral Arctic seas in the past century. A distinct decrease in driftwood incursion during the last 30 years matches the observed decline in pan-Arctic sea ice extent in recent decades. Our new approach successfully employs driftwood as a proxy for Arctic Ocean surface circulation and sea ice dynamics.

Plain Language Summary We present a 500-year history of driftwood arriving to the shorelines of northern Svalbard. Driftwood in the Arctic results from dying trees entering the large rivers that drain the circum-Arctic land masses, which upon flowing into the Arctic Ocean can become locked up in forming sea ice. This enables the wood to travel across the Arctic Ocean without sinking, making it an invaluable proxy for sea ice extent by recording variations in Arctic Ocean surface currents (and therefore sea ice drift) and ice cover. With comparison of tree ring width (TRW) measurements of these driftwood samples to TRW series from trees throughout the boreal forests, we can determine the region each sample came from. We can thus approximate its likely trajectory across the Arctic Ocean. Arctic sea ice is rapidly declining in extent and thickness, with impacts on local and global climatic and ecological conditions. Knowledge of past changes is needed to place this modern trend within a broader context to aid future predictions for Arctic sea ice. Our record matches the observational record of Arctic Ocean surface circulation patterns and climate conditions, supporting the use of driftwood as a proxy for Arctic Ocean surface current and sea ice dynamics.

1. Introduction

The Arctic is vulnerable to climatic changes on a range of temporal and spatial scales from geological to inter-annual, and a hotspot of warming under modern climate change due to the Arctic Amplification (Serreze & Francis, 2006) — a term for the feedbacks and interactions from the region's sea ice and snow cover resulting in enhanced and accelerated greenhouse gas-induced warming in the Arctic. Recent anthropogenic

Project Administration: Marc Macias-Fauria
Resources: Ólafur Ingólfsson, Marc Macias-Fauria
Supervision: Marc Macias-Fauria
Visualization: Georgia M. Hole, Thomas Rawson
Writing – original draft: Georgia M. Hole
Writing – review & editing: Georgia M. Hole, Thomas Rawson, Wesley R. Farnsworth, Anders Schomacker, Ólafur Ingólfsson, Marc Macias-Fauria

trends are well documented by a rapid decline in the extent and thickness of sea ice (Maslowski et al., 2012; Polyak et al., 2010). The continuing decline in sea ice cover is expected to result in wide-ranging consequences impacting the Arctic and beyond. These include impacts on terrestrial and marine productivity, changes to global atmospheric and ocean circulation patterns, increased temperatures and rainfall, terrestrial fauna and flora population fragmentation and habitat reduction, increased marine species interaction and connectivity, and northward expansion of lower-latitude species (Bintanja & Andry, 2017; Bjorkman et al., 2020; Francis & Vavrus, 2012; Macias-Fauria & Post, 2018; Overland & Wang, 2010; Overland et al., 2016; Post & Høye, 2013; Screen & Simmonds, 2010, 2014; Vavrus et al., 2017). The Arctic Oscillation (AO) or Northern Annular Mode/Northern Hemisphere Annular Mode (NAM), is defined as the principal component of extra-tropical Northern Hemisphere sea-level pressure and regarded as the most influential mode of atmospheric circulation and climate variability in the Arctic (Comiso & Hall, 2014; Thompson & Wallace, 1998). Dynamic processes affecting the Arctic Ocean such as the AO are being increasingly examined for their impact on ocean circulation and sea ice dynamics (e.g., Barnes & Screen, 2015; Comiso & Hall, 2014; Ding et al., 2017; Hole & Macias-Fauria, 2017; Rigor et al., 2002). Data on past conditions are needed to understand the region's abiotic and biotic responses to various climatic processes and forcings and their resulting impacts on a global scale (Armand et al., 2017; Dieckmann & Hellmer, 2010). Uncertainties remain on the spatiotemporal dynamics of Arctic sea ice throughout the Holocene, with discontinuous data on sea ice extent, discussed below, prior to the generation of spatially explicit sea ice extent information by satellite observations in the late 1970s (Post & Høye, 2013). The observational record has been extended back in time to the late nineteenth century by compiling various observational data sources including ship reports, airplane surveys, compilations by naval oceanographers and analyses by national ice services (Walsh et al., 2017). Reconstructions of sea ice preceding observations commonly utilize ocean sedimentary core data. Such records are, however, limited in spatiotemporal resolution due to low sedimentation rates in the central Arctic Ocean (Backman et al., 2004; Polyak et al., 2010), limiting their insight into sea ice fluctuations at the sub-millennial scale. Moreover, they generally do not provide direct information on sea ice dynamics. Further knowledge of past sea ice dynamics is therefore needed to understand the context of recent change and gain insight into possible future sea ice trajectories under conditions of increasing global average temperatures.

1.1. The Arctic Ocean and Sea Ice

The extent, area, thickness and dynamics of Arctic sea ice are driven by both thermal and physical dynamics of the Arctic Ocean system, including spatiotemporally variable atmospheric and oceanic heat fluxes, prevailing winds, and ocean currents (Haas & Thomas, 2017). The position of Arctic Ocean circulation patterns is driven by prevailing winds, most notably the upper-ocean anticyclonic Beaufort Gyre (BG) (Timmermans et al., 2018). Together with the Transpolar Drift (TPD), BG, and TPD are the primary circulation systems in the modern Arctic Ocean (Figure 1). Such physical dynamics also influence heat and salinity transport and storage in the Arctic, impacting climate both locally and beyond the Arctic (Carmack et al., 2016).The two systems initiated during the Early Holocene after the closure of the Bering-Chukchi land bridge and opening of the Bering Strait circa 11 ka BP (Bartlein et al., 2015). The BG displays a mean annual clockwise motion in the western Arctic Ocean (Polyak et al., 2010), recirculating and enhancing survival of sea ice within the Arctic basin. The mean residence time for ice in the BG is circa 5 years (Rigor et al., 2002), aiding the formation and preservation of multi-year ice that can reach up to 5 m thickness (Mahoney et al., 2019). The TPD is a surface ocean current running roughly parallel to the Siberian coast and transporting Arctic ice and waters southwards to the North Atlantic through the Fram Strait, favoring the loss of ice. Holocene fluctuations in the extent and orientation of the TPD have been proposed to vary between three overall states (Dyke et al., 1997). These involve lateral shifts from (a) an eastward route toward Fram Strait, with sea ice (and any driftwood entrained in it) advection to the European Arctic; (b) a westward route toward Greenland with sea ice advection to the Canadian Arctic Archipelago (CAA); and (c) a split route with sea ice transport divided between the east and west. A driftwood-based reconstruction of the dynamics of Holocene sea ice extent and dynamics shows that there has been a progression from millennial to centennial shifts in the relative position of the TPD and BG throughout the Holocene, with indications of alignment with concurrent dynamics of the AO (Hole & Macias-Fauria, 2017). The AO Index is characterized as the variable atmospheric mass exchange between the Arctic Ocean and temperate latitudes (Rigor et al., 2002),

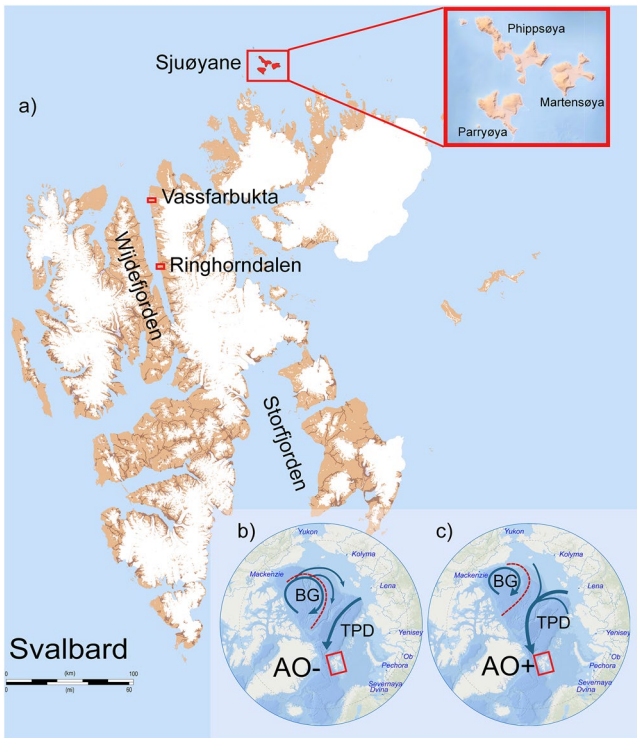

Figure 1. (a) Driftwood sampling locations of Sjuøyane, Ringhorndalen (sampled 2016), and Vassfarbukta (sampled 2018). Insert panel: Two modes of the Arctic Oscillation Index (AO), showing wintertime surface circulation patterns of Beaufort Gyre (BG) and Transpolar Drift (TPD), and the resulting influence on ice residence times. Map figure modified from Norwegian Polar Institute (2014). (b) Low index, negative AO polarity with a strengthened Beaufort Gyre and recirculation of sea ice. (c) High index, positive AO polarity with a weakened BG. The red dashed lines encircle the region of ice recirculation in the BG by the mean sea ice motion field (circulations compiled and modified from Rigor et al. (Rigor et al., 2002)).

with positive or negative polarity determined by anomalies in Sea Level Pressures (SLPs) over the polar regions and mid-latitudes (circa 55°–60°N; Kwok et al., 2013). The AO is a key physical driver of the position of the TPD and the balance between the strength of the BG and TPD circulation patterns (Rigor et al., 2002). The influence and variation in the AO over the Holocene is outlined in greater detail by Hole and Macias-Fauria (2017), including evidence of late Holocene centennial fluctuations in AO index polarity and ocean circulation patterns.

1.2. Sea Ice Observations

Sea ice observations provide information to varying degrees of accuracy, and the observational record encompasses–partially until the advent of remote sensing data–the past ~1,000 years. Since Iceland's settlement in circa 870 CE, records were kept of sea ice incidence by Icelandic fisheries (Polyak et al., 2010), enabling a regional sea ice index for the period 1600–1850 CE to be developed (Ogilvie & Jónsdóttir, 2000). In Svalbard, sea ice information since 1800 has been collected from sealers, ships, and trappers wintering on the archipelago by the Norwegian Polar Institute (Vinje, 2001). April sea ice extent from 1850–1998 has been generated from ship data, aircraft reconnaissance flights, and satellite observation data (Vinje, 2001). In the Barents Sea, April sea ice was recorded by Norwegian ice charts by sealing and hunting expeditions from 1850 to 1949 and 1966 to 2001, and intervening years measured by Soviet reconnaissance aircraft (Shapiro et al., 2003). Sea ice draft and thickness were also measured through upwards sonar data by submarine cruises throughout the Arctic from 1958 onwards (Rothrock et al., 2008). These include comparison of drift data from two summer polar cruises in 1958 and 1970 (McLaren, 1989), before more extensive draft data collection as part of the Scientific Ice Expeditions (SCICEX) program (Gossett, 1996). Since the 1970s, spatially explicit sea ice extent information has been available by the development of satellite observations (Post & Høye, 2013). Using these records, Walsh et al. (2017) produced a spatially explicit pan-Arctic sea ice data set since the late nineteenth century at fine spatiotemporal resolution, enabling a comparison between historic data sets and proxy-based reconstructions (Post & Høye, 2013).

1.3. Using Driftwood to Infer Past Sea Ice Conditions

The geological record and proxy data provide information on environmental and climatic conditions preceding the observational record. Biogenic and inorganic information is gleaned from a variety of biogenic data. Inorganic data include the use of ice-rafted debris (IRD) and radiogenic isotopes for tracking ice drift and provenance (e.g., Fagel et al., 2014; Hillaire-Marcel et al., 2013; Stickley et al., 2009). Biogenic data are collected from ocean sediment cores and include dinoflagellate cysts, ostracods, diatom, and benthic foraminifera assemblages (Cronin et al., 2013; De Vernal et al., 2013; Seidenkrantz, 2013). Highly branched isoprenoid (HBI) lipids produced by diatoms, notably IP_{25} (the ice proxy with 25 carbons; Belt et al., 2007), have also been used for sea ice reconstructions by assessing the relative proportion of sea ice to phytoplankton biomarkers, termed PIP_{25} (brassicasterol, dinosterol or HBI trienes; e.g., Belt, 2018; Müller et al., 2011).

Raised beaches that occur in north-western Eurasia are an evident sign of postglacial adjustment of emergence following the retreat of past ice-sheet loads. Their current elevations result from the balance between eustatic sea level change and isostatic rebound of the lithosphere following the latest deglaciation of northern Eurasian ice sheets (Forman et al., 2004). Such raised beaches in Svalbard often lack vegetation due to their low temperatures, aridity, high alkalinity and low nutrient availability (Dyke et al., 1997; Forman et al., 2004). Such harsh conditions preserve datable driftwood, whalebones and pumice as decomposition is

limited (Blake, 1961; Bondevik et al., 1995; Farnsworth, Blake, et al., 2020; Feyling-Hanssen & Olsson, 1959; Schomacker et al., 2019). Driftwood is the preferred target for analysis in this study due to its terrestrial origin (and therefore radiocarbon dating suitability) and delivery to within 1–2 m above sea level by storm or ice pressure, although it can later migrate shoreward by slope processes (Funder et al., 2011). Driftwood can also be used as a proxy for sea ice extent and dynamics.

Deposits of driftwood on Arctic shorelines reveal the transport by sea ice within large-scale Arctic Ocean circulations, which enables the reconstruction of past surface-current dynamics and sea ice conditions in the Arctic (Dyke et al., 1997; Funder et al., 2011; Häggblom, 1982; Hole & Macias-Fauria, 2017). Up to now, driftwood-inferred sea ice conditions have not been directly compared with the observational record. Reconstructions of past sea ice conditions employing this proxy have been based on an understanding of the conditions required for felled wood in the boreal forest to reach high arctic shorelines. The delivery of driftwood to the shores of Svalbard requires initial entrainment in seasonal sea ice before joining multi-year sea ice for long-distance transport due to its limited buoyancy once waterlogged (Häggblom, 1982). Seasonal sea ice around Svalbard, and therefore seasonally open waters, enable wave action to deliver the driftage to the shoreline (Farnsworth, Allaart, et al., 2020). The incurred driftwood derives from the major rivers that drain the boreal forest regions of North America and Eurasia. The inflow from river runoff at ~3,300 $km^3\ yr^{-1}$ (Alkire et al., 2017), together with precipitation, constitutes the greatest proportion of annual freshwater influx into the Arctic Basin (Serreze et al., 2006). This is followed by the substantial inflow of Pacific water through Bering Strait, which contributes 2,300–3,500 $km^3\ yr^{-1}$ (Woodgate, 2018). In the boreal forest zone, tree-growth is limited by climate, leading to coherent (not individually highly variable) tree-ring growth patterns within broad climatic region/watersheds (Eggertsson, 1993). This coherency, or similarity in individual tree growth patterns, enables regional chronologies of mean tree-ring growth patterns to be created across the boreal forest zone (Schweingruber, 2012) and utilised for dendrochronological matching to driftwood derived from possible boreal source regions. Although the Arctic-draining rivers have been surrounded by boreal forest throughout the Holocene (Hopkins et al., 1981), the Eurasian boreal tree limit in the Early to Middle Holocene of circa 9.5–6 ka BP lay up to 200 km northwards at the circumpolar coastlines (MacDonald et al., 2000).

The geographical distribution of dominant and abundant tree species across the boreal forest (see Hellmann et al., 2013; MacDonald et al., 2008), has been used to infer a genus-based division of driftwood sources to indicate wood provenance. *Larix* (larch) is a markedly common genus of conifers throughout Asian boreal forests and is assumed to indicate a Siberian origin. *Picea* (spruce) is another boreal forest genus of coniferous species very common in North America, and is assumed to signify a North American origin (e.g., Dyke et al., 1997; Eggertsson, 1993; Funder et al., 2011; Häggblom, 1982; Hellmann et al., 2013; Nixon et al., 2016). In North America, *Picea* was present between 10 and 7 ka north of the Mackenzie Delta, up to 70 km north of the modern treeline (Ritchie & Hare, 1971). This resulted from increased summer insolation and temperatures compared to modern conditions (MacDonald et al., 2008), which then migrated to the modern limit at 60–70°N (Bigelow et al., 2003; Sokolov et al., 1977). The boreal forest reached its current composition by irca 6 ka BP in Canada (Tremblay et al., 1997), and by 3–4 ka BP in Eurasia (MacDonald et al., 2000), with increased *Larix* occurrence during 10–3.5 ka BP.

For more spatially precise provenance determination, dendrochronology and tree ring width (TRW) analysis has proved a vital tool in dendroarchaeological efforts (Taylor & Aitken, 1997) and Arctic climatic and environmental reconstructions (Koch, 2009; Owczarek, 2010). Past driftwood dendrochronological studies have considered only reference chronologies associated with a particular drainage basin (Eggertsson, 1993; Eggertsson & Laeyendecker, 1995) based upon consideration of Arctic surface currents. However, recent studies have highlighted that such assumptions can be incorrect, and a far wider extent of circumpolar sites must be considered during such processes, to accurately capture the potential history of samples (Hellmann et al., 2013). A recent combined assessment of radiocarbon and dendrochronological age estimates of Arctic driftwood samples found that radiocarbon dates from buried driftwood were in agreement with dendrochronological dating of modern beach ridge systems in coastal eastern Siberia (Sander et al., 2021), thus supporting the validity of age indications obtained from driftwood found on Holocene beaches.

The aim of this paper is to utilize Arctic driftwood collected from modern shorelines to create a proxy-based reconstruction of regional sea ice conditions and Arctic Ocean circulation dynamics at a decadal resolution,

and to evaluate inferences made from naturally felled driftwood material against the observational record. In this study we provide a 500-year record of driftwood incursion onto northern Svalbard modern active shorelines. TRW series and genus information are determined for the samples where possible, before cross-dating with reference chronologies from the circum-Arctic boreal forest zone to determine the climatic regions/watersheds the driftwood originated from. As sample cross-dating may result in a wide range of possible matches across the pan-boreal region and possible bias towards the regions covered by reference chronologies, our study includes a new approach to select most probable origin sites from multiple cross-dating matches and visualizing these results through spatiotemporal density plots. The resulting spatiotemporal distribution of best matches for all samples provides a 500-year time series of driftwood delivery to northern Svalbard, enabling a proxy-based reconstruction of Arctic Ocean surface current and sea ice dynamics over this period. Our study tests for the first time the validity of Arctic driftwood as a proxy for sea ice dynamics at high spatial and temporal resolutions by directly comparing driftwood-inferred sea ice information against other reconstructions and the observational record.

2. Methods

2.1. Sampling Sites

The raised beaches on the Svalbard archipelago are ideal for preserving stranded driftwood. Svalbard is located at the proposed north-western part of the Late Weichselian Svalbard-Barents Sea Ice Sheet (SBSIS), with abundant preserved raised beach sequences reflecting the pattern and rate of relative sea level changes on Svalbard in response to the deglaciation of the SBSIS (Forman et al., 2004; Ingólfsson & Landvik, 2013). Samples were collected in August 2016 and July 2018 from three localities from the northern coastline of the Svalbard Archipelago. In 2016, driftwood was collected from the three largest islands of Sjuøyane (Martensøya, Phippsøya and Parryøya), and Ringhorndalen in Wijdefjorden, Spitsbergen. During a 2018 field campaign to Vassfarbukta in Wijdefjorden, Spitsbergen, a total of 30 driftwood samples were collected between the active beach face and the storm berm up to irca 4 m above mean sea level along a 200 m stretch of coast. All sampling locations were expected to capture driftwood from the same large-scale ocean currents (Figure 1). On Sjuøyane, the lowlands above the marine limit are covered by glacial drift of angular to subangular cobbles and boulders, within a silty/clayey matrix. In this matrix there are abundant shell fragments, likely incorporated by glaciers originating from Nordaustlandet that also supplied erratics of granites and quartzites (Forman & Ingólfsson, 2000). Holocene arrival and incursion of driftwood onto Sjuøyane and Wijdefjorden is influenced not only by broader ocean circulation dynamics and sea ice conditions, but also by local deglaciation patterns and geomorphology. Dating of driftage deposits and preserved regressional strandlines indicate that deglaciation of Phippsøya occurred before circa 9.4 ka ago (Forman & Ingólfsson, 2000). The relative sea level fell to less than current sea level circa 9–7 ka BP, before a transgression rising sea level to above present levels at circa 6.2 ka BP indicated by cross-cutting beach ridges, and observed in other marginal foreland records around Svalbard such as a whalebone dated to circa 6 ka BP found at 5 meters above high tide (mean high tide mark (m a.h.t.)), behind the modern storm beach of Kongsfjorden (Forman et al., 2004). Similar scales of isostatic readjustment and relative sea level changes patterns occur in northern Wijdefjorden (Farnsworth, Allaart, et al., 2020; Forman et al., 2004; Schytt et al., 1968). The impact of such dynamics on driftwood incursion is minimal for this study, due to our aim to target samples from the modern shoreline for reconstruction of sea ice conditions over recent centuries, and for the comparison of modern sample spatiotemporal distribution with observed circulation patterns and sea ice dynamics in the Arctic Ocean during the last 120 years.

2.2. Field Sampling Methods

A total of 95 driftwood samples were collected from Sjuøyane, Vassfarbukta, and Ringhorndalen shorelines and raised beach terraces where samples were deemed in-situ. The datum for raised beach elevation measurements is the present, m a.h.t., seen at the coastline as a swash limit (Forman et al., 2004). The storm beach elevation can reach over 4 m on bays exposed to direct storm fetch (Forman, 1990; Zeeberg et al., 2001) and this can carry washed up material substantially above the sea level of the time, giving uncertainties to dating by local geomorphology for raised-beach samples. At all sites, naturally felled driftwood at the modern shoreline was targeted by the sampling of logs exhibiting intact root stock. These driftwood

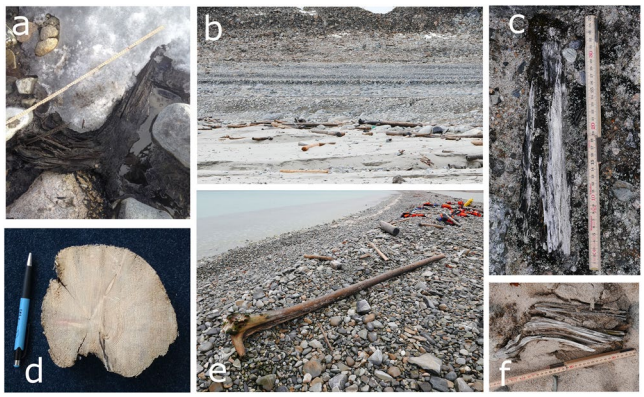

Figure 2. Range of preservation level of driftwood samples on Sjuøyane. Ruler placed for scale in panels (a, c, and f), and pen placed for scale in dry driftwood disc in panel (d). Samples along the modern shoreline have the highest levels of preservation, with intact trunks and visible tree-ring series allowing dendrochronological analysis. Only samples that had sufficient preservation of tree rings and that preserved their root structure–and thus were likely naturally felled–were used to create our sample data set (such as panels (b, d, and e)). More degraded samples such as in panels (a, c, and f) did not have sufficiently preserved rings to be included in the data set.

logs were sub-sampled at peak thickness with a saw, where sub-sampled slices exhibited the maximum amount of intact tree-rings (Figure 2). For elevation calculations, handheld GPS devices were used with occasional DGPS or altimeter data. Older driftwood was sparse, with most found ≤7 m a.h.t., and the majority of the samples are from the modern shoreline. The driftwood sampled varied in condition; more recently deposited driftwood samples (e.g., Figure 2d) had intact tree rings that were suitable for analysis.

2.3. Laboratory Processing

Driftwood samples were assessed for viable tree ring series, with 59 of the 95 samples suitable for measurement and analysis. Of the 59 driftwood subsamples from northern Svalbard, 27% (16) were from Sjuøyane, while 73% were from Wijdefjorden ($n = 28$ and $n = 15$ from Ringhorndalen and Vassfarbukta respectively). These were then sanded using drill-mounted sanding bands, and annual ring widths of each sample were measured to 1/1,000 mm accuracy using LINTAB tree-ring measurement table and TSAP-Win Professional version 0.89 (Rinn, 2003). Where possible, the genus of the driftwood samples was identified by microscopy through examination of stained radial, tangential, and longitudinal sections.

In the majority of dendrochronological studies, reference chronologies are limited to a specific temporal and geographical range based upon the context of the samples taken, be it by pre-existing knowledge of logging activity (Drake, 2018), or sapwood estimation (Daly, 2007; Hughes et al., 1981). Once a reference subgroup is determined, the "best match" is then identified as that with the highest *t*-value, a statistical measure of a sample's similarity to a period in the reference chronology. Identifying such reference subgroups is a more difficult process when investigating naturally felled driftwood origins. The measured tree-ring series were cross-dated both visually by comparison of ring-width marker ring lists and by use of the chronology-building statistics of TSAP-Win software. Tree ring series were amassed and standardised to remove non-climatic trends such as ontogenetic growth and competition effects using a two-part trend elimination (Cook & Peters, 1997). First, a negative exponential curve was fitted, before taking the residuals. Second, to completely remove multi-year variance, a 5-year moving average was applied, with the resulting residuals then taken. This was undertaken to remove autocorrelation (year-to-year variance) to facilitate the computation of correlation coefficients. At least two radii per driftwood disc were measured and combined through a bi-weight robust estimate of the mean to form one chronology per sample.

2.4. Chronology Building–Driftwood Floating Chronologies

The 59 samples with sufficient measured time series were cross-dated using TSAP-Win using a variety of statistical parameters, discussed below. Multiple scoring metrics have been utilized in assessing between-TRW time series similarity. A t-statistic is commonly employed to compare a sample set against a reference chronology. TRW data are standardized by converting to a percentage of the mean of the five ring widths of which it is the center value, which ensures the data have bi-variate normal distribution. The resulting values are then normalized by taking the natural log of percentage figures (Baillie & Pilcher, 1973). This de-trended value is referred to as T-value Baillie-Pilcher (TVBP), however the measure lacks descriptive power in the absence of extreme ring-differences between chronologies. For cases with less extreme ring-differences, the Gleichläufigkeit (Glk) parameter (or concordance coefficient) is also employed, which instead assesses similarity of sample slope intervals (Eckstein & Bauch, 1969; Schweingruber, 2012). To capture the strengths of both metrics, we considered the Cross-Date Index (CDI) within our study, provided by the TSAP-Win package (Rinn, 2003). CDI gives the quality of agreement between sample series by combining the Glk measure of overall accordance of two series with the t-value measure of the correlation significance:

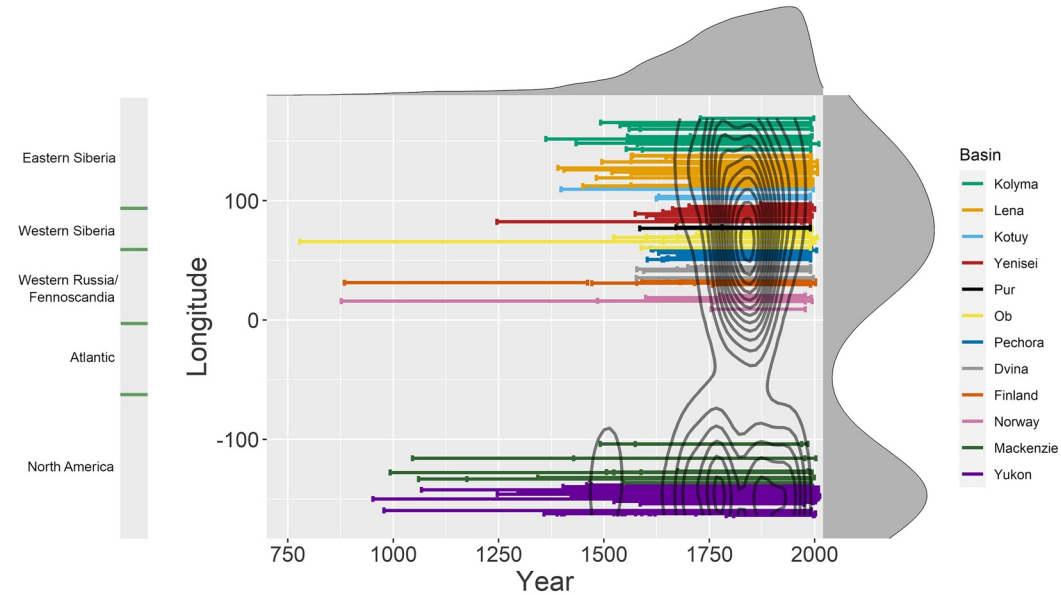

Figure 3. Spatiotemporal distribution of 222 reference chronologies from across the Eurasian and North American circum-Arctic boreal forest zone, sourced from the International Tree Ring Data Bank (ITRDB, http://www.ncdc.noaa.gov/data-access/paleoclimatology-data/datasets/tree-ring) (Grissino-Mayer & Fritts, 1997). Each line represents a single chronology, depicting the longitude and timespan covered, with line colors depicting the river basin/longitude of each chronology. The longitudinal density plot is directly calculated from the plotted longitudes, and the top density plot captures the number of chronologies that include the respective year. The overlaid contour plot is mapped using the longitudinal and time range midpoint data for each chronology.

$$\mathrm{CDI} = \frac{\left(\mathrm{Glk} - 50 + \left(50 \times \sqrt{\frac{\mathrm{overlap}}{\max \mathrm{overlap}}}\right)\right) \times t - \mathrm{value}}{10} \quad (1)$$

With the inclusion of both Glk and t-value in the above equation, CDI captures the magnitude of both measures. Therefore, the CDI gives a date index of possible series matches (Rinn, 2003). Significant correlation was set to Glk > 60%, TBP > 3.0 and a CDI ≥ 10 (Rinn, 2003). The cross-dating of series within the chronologies was examined using the COFECHA-style Cross-Date Check feature of TSAP-Win (Holmes, 1983). Any series or segments of series that did not surpass sufficient cross-date parameters were removed. Successfully cross-dated individual series were combined to floating chronologies.

2.5. Reference Chronologies From the Boreal Forest

Reference chronologies from the circum-Arctic boreal forest zone were sourced from the International Tree Ring Data Bank (ITRDB, http://www.ncdc.noaa.gov/data-access/paleoclimatology-data/datasets/tree-ring) (Grissino-Mayer & Fritts, 1997). Individual, dated TRW measurement series used to form locality reference chronologies were downloaded before undergoing the same detrending process as driftwood samples. These dated series were then formed into chronologies via the TSAP-Win chronology building tool. The spatiotemporal spread of these reference chronologies (Figure 3) provided possible age and source data for crossdating with each driftwood sample.

2.6. Data Analysis

Floating driftwood chronologies were compared with all available boreal forest reference chronologies in order to determine their most probable origin. In a first approach, all matches considered viable by TSAP-Win (CDI ≥ 10) were plotted to display and investigate the spatiotemporal trend of matches, providing the density plots of the longitude and felling dates of all potential matches. However, since we consider a

pan-boreal reference chronology, there is a risk of over-representing the geographic regions and time-periods that are better constrained by our reference chronology. That is, a sample may be more likely to match to a period/region for which there are more reference chronologies available. Each chronology within our reference chronology data set was examined by the longitude and timespan covered (Figure 3). The gray-shaded y-axis density plot displays the geographic distribution represented, while the x-axis density plot depicts the abundance of chronologies associated with each individual year. The geographic distribution is approximately represented evenly between the two key landmasses of the northern hemisphere (North America and Eurasia). More recent years are better represented by our reference chronology due to the reliance of the database on the collection of reference chronology data, which is more abundant in recent centuries. Information from several centuries ago is restricted to a few individual chronologies, with a marked dearth of data from ~1000 to 1500 CE in eastern Siberia.

Other dendrochronological studies that have considered a wider potential source region have demonstrated a wide range of t-value matches, which would all have been considered a sign of good-fit by more restrictive references (Daly, 2007; Daly & Nymoen, 2008). Such studies will still routinely use the highest *t*-value as a measure of the most probable origin, however such approaches risk bias toward regions with better developed reference chronologies. Based upon this, we computed a new metric (Weighted Score) to help determine the most likely match within our results for each sample. This was achieved through weighting the CDI scores by the inverse of the density plots in Figure 3. As such, matches that were considered more "unlikely" by appearing in less-reported regions and time periods of the reference chronologies were rewarded. A new reference score was constructed for each potential match representing the initial CDI scores, corrected by the overall reference chronology spans, and increased by the number of identical temporal matches for the sample, that is:

$$\text{Weighted Score} = \text{CDI} \times \frac{\left(\text{Total number of matches with the same timespan}\right)}{\text{Reference chronology densities for the match}} \tag{2}$$

A match was considered better if it had a higher CDI. Additionally, matches to a poorly represented region in the reference chronology were weighted positively. We constructed linear interpolations of the reference chronology densities (Figure 3) via the *approxfun* function within R. This produced two functions, $f_{\text{time}}(x)$, $f_{\text{long}}(y)$, which provide the relative densities for a given year x, and longitude y. We then calculated the new score for each match as:

$$\text{Weighted Score} = \frac{\text{CDI} \times n}{f_{\text{time}}\left(x\right) \times f_{\text{long}}\left(y\right) \times \sum^{\text{matches}} \text{CDI}} \tag{3}$$

where x and y are the start-date and longitude of the match in question, respectively, and matches is the total number of matches for the sample with the same start/end dates. n is the total of all match CDIs for the sample. In order to determine the 'best match' for each sample, the CDI values and Weighted Score values were examined, with high CDI values showing high Weighted Score values considered a sign of a good match. A decision workflow was employed when assessing the matching parameters (Figure 4). With all data available, the match values of CDI and Weighted Score were chosen. If there was a cross-date match with sufficiently high CDI and/or Weighted Score, a match was chosen, with a preference to the Weighted Score in case of doubt. Additional information was employed to assess the uncertainty in the choice of the best match. Chronology density plot surfaces, the presence of multiple matches for a common date and region, and genus agreement between sample and reference chronology, as well as visual comparison between floating and reference TRW chronologies, were considered for match choice. Additional information was not used to determine a match but could be used to gain confidence on the chosen match or to decide that either the existing match had high uncertainty or that there was not enough information to determine a match (Figure 4). CDI scores, Weighted Scores and match choices are available in Data Set S2. All match distribution plots for samples can be seen in the Data Set S2. All data processing, visualization and score calculations were performed in *R* utilizing the *tidyverse* suite of packages. All data and code used is made freely available at https://osf.io/z4t3a/.

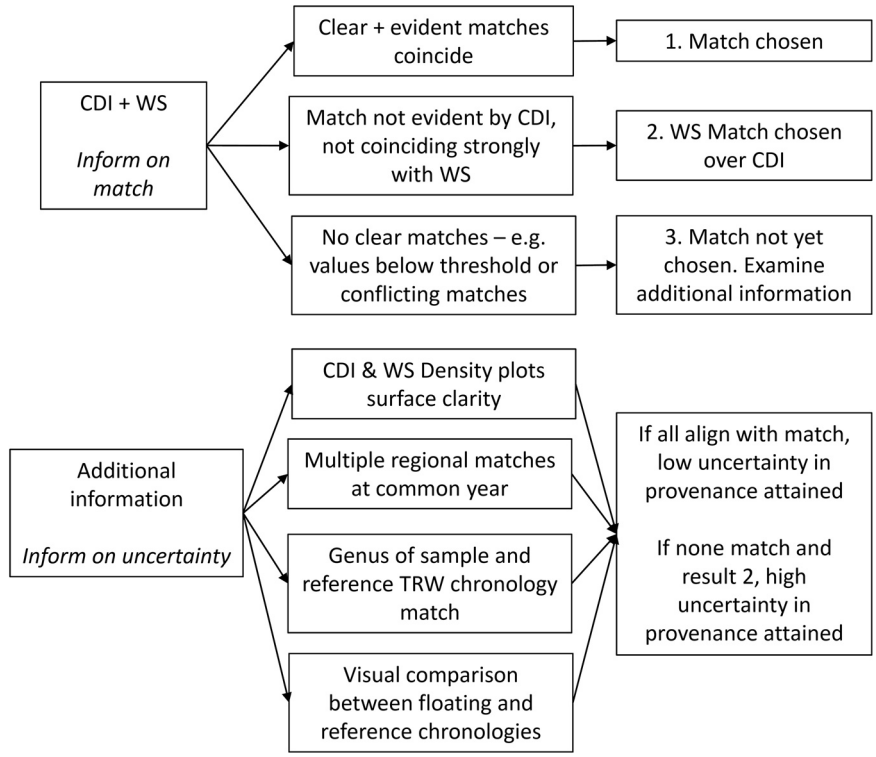

Figure 4. Decision workflow for the determination of cross-dating matches between samples and reference chronologies from the International Tree Ring Data Bank (ITRDB). WS = Weighted Score.

3. Results

Match plots are available for all samples in Data Set S2. Plots for two contrasting samples (RIN24 and RIN28) are provided as an example in Figure 5. RIN24 exemplifies a low uncertainty provenance case, whereas RIN28 exemplifies a sample with higher uncertainty where a match is obtained by Weighted Score supported by multiple regional matches. Each point on the plot represents a potential match, where the color of the point shows its associated drainage basin, and the size of the point represents the CDI value of the match. The density plots provided were constructed based upon the respective x and y value of each point and are weighted by the CDI value. RIN24 (segment length = 58 years) correlated very clearly with reference chronologies from the Yukon basin, and its most recent year was determined as 1831 CE, showing the highest similarity with a reference TRW chronology named "Frost Valley." In contrast, RIN28 (segment length = 78 years) had a higher number of possible matches. Taken individually, the highest t-value (or CDI value) suggested the best match depicts a fell date of 2007 from the Lena River region (blue-outlined circle and arrow; Figure 5a), longitude 123.36, with a CDI of 36. However, this match is isolated: sample RIN28 showed a high CDI value with one reference chronology only, despite the abundance of chronologies that encompass the year 2007 in the reference data set, including several in the Lena River drainage basin. This suggests that such value might be due to chance. The year with the most concordance of common date matches is plotted in red, in this case 1701 and 1865 with 7 matches for each date (Figure 5c). The contour plot surfaces computed using unweighted CDI values (Figure 5a) suggested the best match would be in the late 1800s from the Ob region. By utilizing the Weighted Score metric, factors were judged together to assess the most probable match in the face of all available data, which was determined to be a match to an end date of 1701 from the Yukon region, via the "Bye Rosanne/ak061" reference chronology in Alaska (highlighted with a blue-outlined circle and arrow in Figure 5b). All best matches and weighted scores, with rationale behind match choices via this method, are available in Data Set S1.

The spatiotemporal distribution of best matches for all samples collected were assessed for distribution trends (Figure 6). Multiple matches were included when a sample resulted in more than one possible

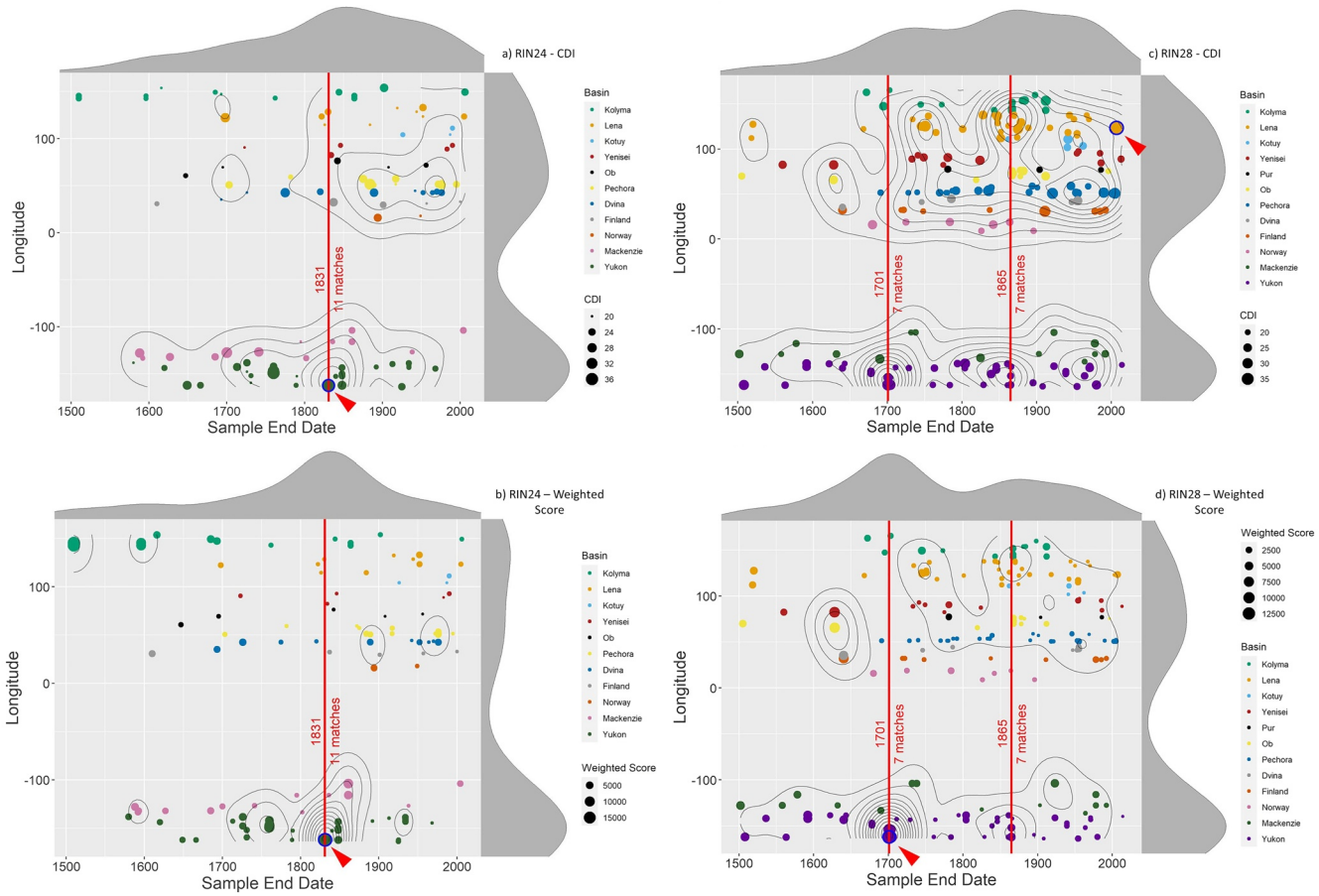

Figure 5. All potential matches for samples RIN24 (a and b) and RIN28 (c and d) using the scores Cross-Date Index (CDI) and Weighted Score, demonstrating two examples of the employment of the decision workflow. Each point represents a match to a chronology with the chosen best match denoted by blue circle and red arrow. The color of the point displays the associated drainage basin, and the size of the point represents the CDI of the match in the upper plot and the Weighted Score in the lower plot. The density plots and contours depict the densities of the associated time and longitude axes, weighted by the scores of the matches.

matching chronology (this was only required for one sample, which indicated 2 possible best matches–RIN40). The CDIs for each match were utilized for assessment of the distribution trends, due to the inter-sample comparability, whereas the Weighted Scores values consisted of a more variable magnitude making comparison between samples less useful than comparison of scores per sample. Best matches divided by sampling locality (Sjuøyane, Ringhorndalen, and Vassfarbukta; Supporting Information S1) showed a consistent trend across the three localities, with no distinct variation of driftwood age, provenance, or species. Segment lengths of series ranged from a minimum of 34 to a maximum of 281 years (Figure S1.1). Samples with greater segment length had more likelihood of cross-dating success with reference chronologies, and thus only a proportion of the samples were expected to be successfully cross-dated and therefore have a provenance determined. Regional density plots depicted the distribution of driftwood provenance through densities of the associated time and longitude axes, weighted by the CDI of the matches (Figure 7), which were consistent with the regional divisions (Figure 6). Examination of the spatiotemporal distribution of these samples reveals centennial-scale shifts in the contributing sources of Arctic Driftwood to northern Svalbard. Shifting patterns in the regional density plots indicate increases from Western Siberia over the last two centuries, with smaller centennial variability in North American driftwood delivery. There was a peak in overall driftwood delivery centered around the nineteenth century, an early drop in driftwood delivery from the Barents Sea starting in mid-nineteenth century, increased driftwood delivery in the Siberian shelf during mid-twentieth century, and a synchronous decrease in driftwood delivery to northern Svalbard in the recent decades (Figure 7). The main sea ice features inferred from driftwood incursion to Northern Svalbard in this study are summarized in Table 1 and will be discussed in the following section.

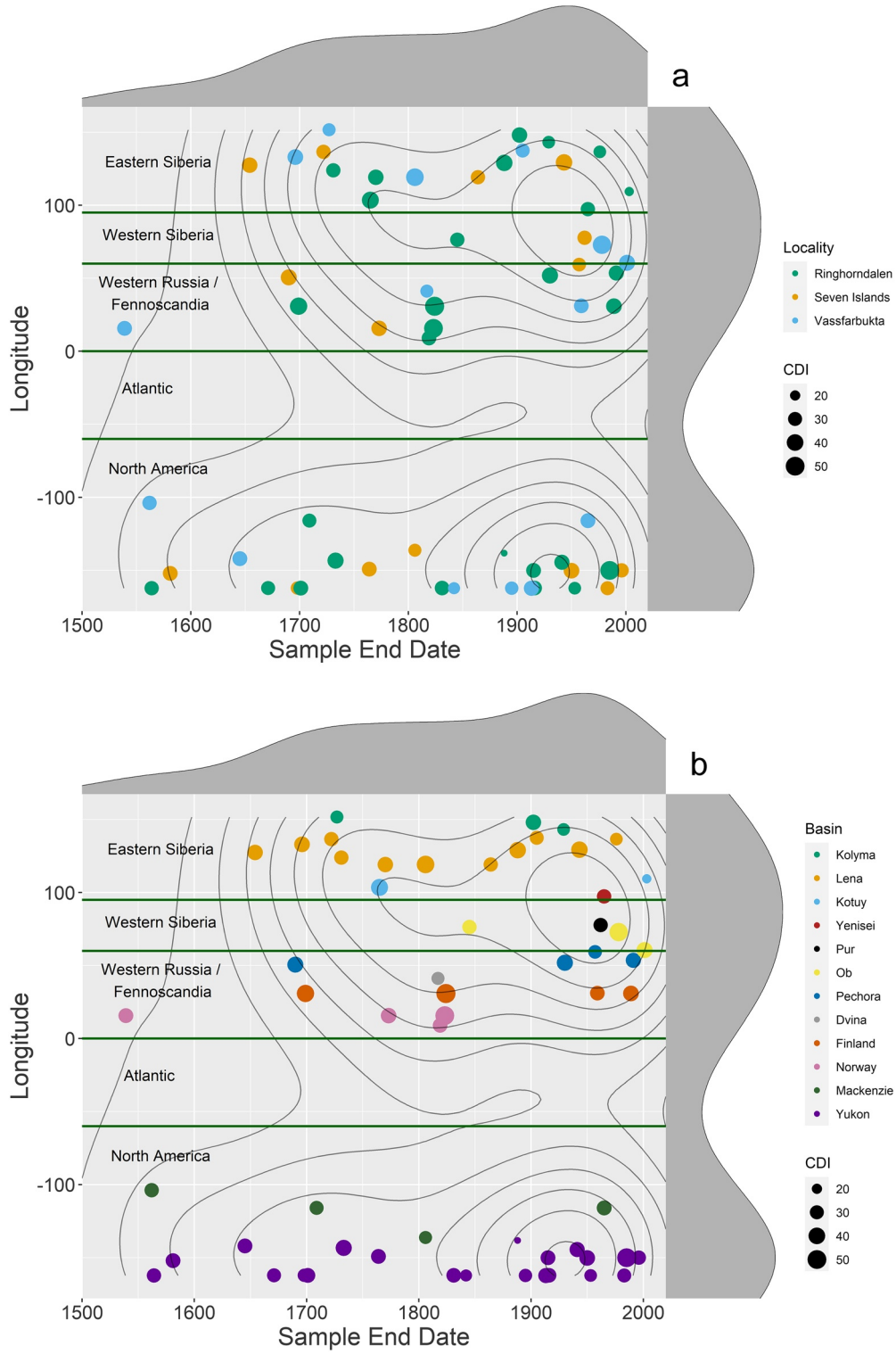

Figure 6. Plot of best matches for all samples. Each point represents a sample's best match to a chronology, with both matches included when a sample shows two possible matching chronologies (1 case–RIN40). (a) The color of each data point corresponds to the sampling site and the size of the point represents the Cross-Date Index (CDI) of the match. (b) The color of each data point displays the associated drainage basin, and the size of the point represents the CDI of the match. The density plots depict the densities of the associated time and longitude axes, weighted by the CDI of the matches. Contours depict the unweighted densities of the spatiotemporal spread of the matches.

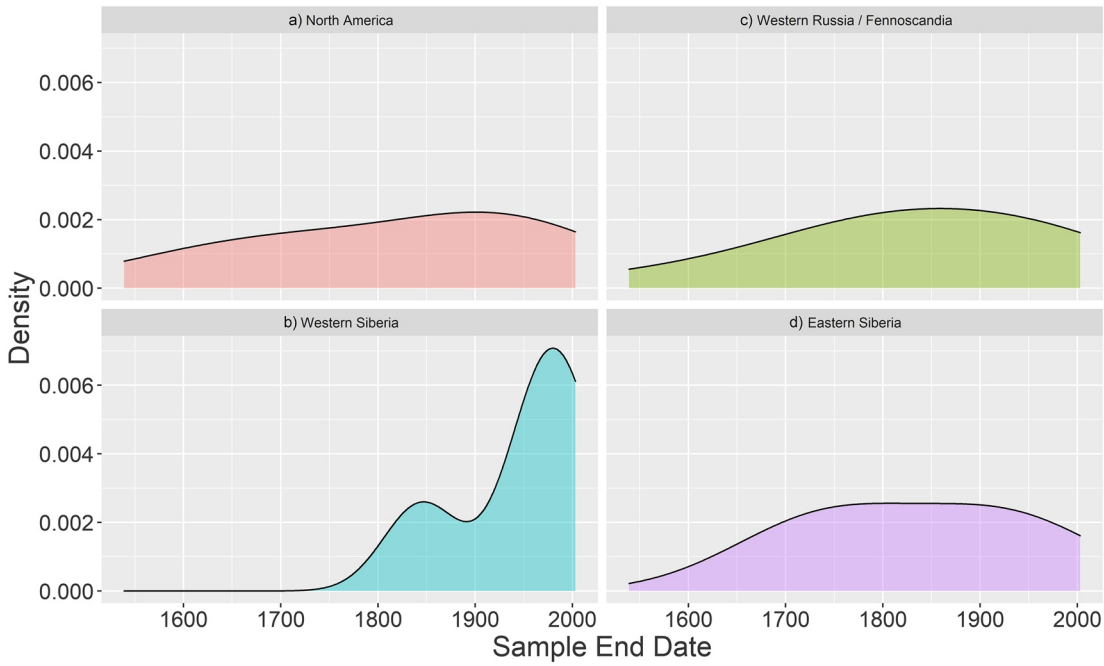

Figure 7. Plot of best match density plots for the four regions (a) North America, (b) Western Siberia, (c) Western Russia/Fennoscandia, and (d) Eastern Siberia, matching regions shown in Figure 6. The density plots depict the densities of the associated time and longitude axes, weighted by the Cross-Date Index of the matches.

4. Discussion

The best matches and regional density plots from our model show that the proportion of Siberian driftwood arriving in Svalbard was greater than that from North American regions as a whole (Figures 6 and 7; Table 1), as expected due to a greater number of boreal zone-draining rivers. These findings agree with both observations of felled and logged driftwood transport (Hellmann et al., 2017) and modeling of driftwood transport based on sea ice velocity, concentration and the sea surface current velocity (Dalaiden et al., 2018). Within North American samples, Yukon River basin dominates over Mackenzie River basin origin. This is expected given the overall direction of the eastward-flowing coastal current at the Mackenzie River mouth, that will tend to divert driftwood toward the Canadian Arctic Archipelago (Dyke & Savelle, 2000): This result gives confidence in the dendro-provenancing methodology employed in this study. A lack of samples of Siberian origin arriving before 1650 CE correlates to the period of low Arctic sea ice cover that spanned the sixteenth and early seventeenth centuries (T2 in the multiproxy reconstruction by Kinnard et al., 2011, that did not employ driftwood; Table 1). A lack of driftwood arriving from Western Siberia before the twentieth century may indicate a lack of sufficient ice in the Kara Sea, although there is no evidence of this in other palaeo-records (Table 1). Another possibility is the Kara Sea acting as a closed system not delivering driftwood to the TPD, which aligns with observed strong closed summer anticyclonic circulation in the Kara Sea, associated with river runoff (Panteleev et al., 2007). Driftwood delivery (and thus inferred sea ice extent) increased markedly in the subsequent ~150 years (again, in line with Kinnard et al., 2011), with a mixed arrival of both Eurasian and North American driftwood between 1700 and 1850 CE, suggesting a well-developed BG able to deliver North-American wood to Svalbard entrained in the TPD. This indicator of cold conditions and multi-year sea ice aligns with inferred late Holocene sea ice increases via a proxy-based sea ice reconstruction including sediment core IP_{25} data from northern Wijdefjorden, Svalbard (Allaart et al., 2020). In that reconstruction, continuous increase in IP_{25} concentrations after circa 0.5 cal. ka BP, in combination with decreased water temperatures and the increased IRD, were inferred to indicate increase in sea ice and cold conditions correlating with the onset of the Little Ice Age (LIA). That record aligns with this study's inferred sea ice increase and well-developed BG after 1650 CE. Cooling in the Barents Sea at circa 1650 CE is also recorded by a cooling period between circa 1650 and 1850 CE based on oxygen isotope analysis and benthic foraminiferal assemblages (Wilson et al., 2011). Cool temperatures are

Table 1
Summary of Comparison of Main Sea Ice Inferences Resulting From This Study With Existing Proxy-Based Reconstructions and Observational Data

Sea ice inference from driftwood	Corresponding reference	
Pre 1650 CE *Observation*: general lack of driftwood from Siberia. *Inference*: low sea ice in Siberian seas.	T2 in Kinnard et al. (2011).	
1700–1850 CE *Observation*: marked increase in driftwood delivery from all sources. *Inference*: more sea ice generally.	Allaart et al. (2020); Kinnard et al. (2011).	
1650–1850 CE *Observation*: abundant driftwood delivery from the Barents Sea. *Inference*: more sea ice in Barents Sea.	Voronina et al. (2001). Cool T in Southern Barents: Mette et al. (2021). Figure 19 in Smedsrud et al. (2013). Cooling in Western Barents in LIA: Wilson et al. (2011).	**Proxy-based data**
1750–1900 CE *Observation*: lack of driftwood from E-Siberia. *Inference:* either very strong BG OR more sea ice in Barents region dominating transport.	More Barents sea ice: Mörner et al. (2020); Zhang et al. (2018). Cool T in Southern Barents: Mette et al. (2021).	
After 1850 CE *Observation*: *reduced driftwood delivery from the Barents Sea*. *Inference*: *less sea ice in Barents Sea, resumed in mid-20th century, but not noticeable close to Norway (western Barents Sea)*.	Divine & Dick (2006); Shapiro et al. (2003); Vare et al. (2010); Walsh et al. (2017).	
Pre 1900 CE *Observation*: lack of driftwood from W-Siberia — the dip in the 20th century (Figure 6) is due to 1 sample only in ~1850 CE. *Inference*: closed Kara Sea system not delivering much to the TPD OR lack of sufficient sea ice in the Kara Sea.	Kara sea has variable circulation driven by wind more than thermohaline: Pavlov and Pfirman (1995). Strong closed anticyclonic circulation associated with river runoff — a prominent feature of the Kara Sea dynamics in summer: Panteleev et al. (2007). No evidence of low sea ice in the Kara Sea during this period — discarded.	**Observational data**
~1940–1980 CE *Observation*: abundant driftwood delivery from Eurasia. *Inference*: abundant multiyear sea ice circulation from Eurasia in mid-20th century: abundant thick ice with a circulation that fed to the TDP.	Sea ice extent: Walsh et al. (2017). Lack of reference observations for driftwood-based inference on sea ice circulation.	
~1900–2000 CE *Observation*: more driftwood variability from Eurasian than from North American sources. *Inference*: overall more variability of sea ice in the Siberian Seas, with more changes regarding multiyear sea ice in these regions during much of the 20th century (except the last decades of the 20th century — see below).	Figure 11 in Walsh et al. (2017).	
~1980–2012 CE *Observation*: drop in driftwood delivery from all sources. *Inference*: sea ice decline overall pan-arctic in the last decades.	Figure 11 in Walsh et al. (2017).	

also indicated ~1705–1824 CE based on southern Barents Sea $\delta^{18}O$ shell-temperature reconstruction (Mette et al., 2021). A reconstruction of annual sea ice persistence from the southern Barents Sea from dinoflagellate cyst assemblages indicates longer sea ice season after 1650 CE (Voronina et al., 2001). A combination of that reconstruction with other proxy-based reconstructions of Barents Sea air-ice-ocean variability also indicates cool conditions during the last ~300 years (Smedsrud et al., 2013).

There is a notable halt of Western Russian/Fennoscandian driftwood delivery after 1850 CE (Figure 6; Table 1). For this material to arrive on the northern shores of Svalbard, sea ice is required in the Barents Sea which will carry it north/north-eastwards toward the Arctic Ocean before joining the TPD. Driftwood from north-eastern Europe returns in the mid-twentieth century, whereas driftwood originating from Norway is constrained to the period 1650–1850 CE, indicating sea ice in the southern Barents Sea at this time and a lack thereafter. This aligns with analysis of a continuous observational record of April ice edge in the Barents Sea, which indicates a retreat in the winter mean ice edge position since 1850 CE (Shapiro et al., 2003). This also correlates with a reduction in sea ice occurrence and north-easterly retreat of the ice edge during this time (Divine & Dick, 2006; Vare et al., 2010). There is a lack of driftwood originating from the most eastern Siberian sources such as the Kolyma basin between 1750 and 1900 CE. This may be indicative of the trajectory of such distal driftwood sources. Given the mean residence time of ice from North America and far-eastern Russia region is circa 5 years (Rigor et al., 2002), there is the possibility of entrainment into the BG disrupting travel to northern Svalbard, or sea ice formation focused in the Barents Sea region, favoring driftwood delivery from this region before 1850 CE.

Further information from direct observations of sea ice dynamics is available since mid-nineteenth century and can be compared to the driftwood record to assess the accuracy of driftwood temporal distribution reflecting the known conditions of the time (Table 1). A composite historical record of Arctic sea ice margins from 1870 to 2003 CE shows a trend of northward and eastward retreat in seasonal ice from 1900 CE onwards, with acceleration of seasonal and annual ice retreat during the last five decades with spatially variable sea ice distribution changes across the Arctic (Kinnard et al., 2008). There is further evidence of such conditions favoring reduced ice, with atmospheric warming driven by enhanced atmospheric and ocean heat transport from the North Atlantic into the region from 1900 to 1940 CE (Bengtsson et al., 2004; Vinje, 2001). The decline in driftwood arriving to northern Svalbard from Western Russian/Fennoscandian sources after the 1850s may be an indication of a reduction of sea ice in the Barents Sea in this period, as indicated by a sustained reduction in March and September ice extent from 1850 to 2013 CE (Walsh et al., 2017). The increase in September sea ice during the late mid-twentieth century is seen in a peak in Western Siberian driftwood delivery in the latter half of the twentieth century, in contrast to decreases for other regions (Figure 7b). A relative maximum is reached by the 1970s within a framework of strong decadal and multidecadal variability on a regional basis, indicating the favoring of proximal sources of driftwood from Eurasian coasts in this period. The steady–even centennial–increase in the delivery of North American driftwood until the last several decades (Figure 7a) likely reflects a more stable (i.e., less variable) source of driftwood in recent centuries. This observation is in agreement with a higher occurrence of sea ice variability in the Eurasian peripheral Arctic seas (most notably the Barents Sea) compared to the Beaufort and Chukchi Seas until late twentieth century (Walsh et al., 2017). As a consequence, increases in the overall frequency of North American wood delivery in Svalbard can signal, depending on the context, lack of sea ice in the Eurasian peripheral seas.

Finally, there is a distinct decrease in driftwood incursions during the last 30 years from each region of our study (Figure 7; Table 1), suggesting a lack of sufficient multi-year sea ice throughout the Arctic to raft driftwood to Svalbard shorelines, matching the record of systematic decrease in pan-Arctic sea ice extent since the 1970s (Walsh et al., 2017). For the period 1990–2003 CE, synthesized historical sources and satellite data show the trend continues with an Arctic-wide retreat of the summer (i.e., multi-year/permanent) sea ice cover resulting in a net increase in the extent, and a northward migration of seasonal sea ice from the peripheral seas, with earlier sea ice retreat in the Barents Sea and a later onset in the Beaufort and Chukchi Seas (Kinnard et al., 2008; Walsh et al., 2017). This spatial shift is matched with multi-year ice loss and replacement with first-year ice, with resulting reduction in driftwood-carrying potential expected to affect the most recent driftwood incursion rates. The most recent driftwood samples, comprised of three samples matched to dates from 1991 to 1996 (Data Set S1), originated from eastern Eurasia and the Yukon drainage basins. Based on the average travel time of up to 7 years for Arctic driftwood (Häggblom, 1982), these recent driftwood samples suggest a reduction in the influx of driftwood during this period. However, there are not enough data points to robustly support this conclusion within the context of the observational record. The lack of naturally felled driftwood arriving to our study site more recently than 1996 CE is remarkable, especially given the ample availability of reference dendro-chronologies since the 1990s in this study.

These centennial-to decadal-scale shifts in source regions for driftwood incursion to Svalbard align with the high variability and high frequency shifts in the TPD and BG strength throughout the late Holocene and associated fluctuating climate conditions, as found in a previous driftwood-based reconstruction of Holocene Arctic Ocean surface current and sea ice dynamics (Hole & Macias-Fauria, 2017). A recent study of 380 driftwood samples collected on eastern and south-western Svalbard (Linderholm et al., 2021) found a dominance (87%) in driftwood originating from northern Russia, with samples dated to the nineteenth and twentieth centuries which were periods of high logging activity in Russia. The study incorporates logged wood which is subject to anthropogenic influence on trends that reflect the logging activity at the time of their harvesting (Hellmann et al., 2016). Therefore a direct comparison is not applicable to our spatiotemporal record, which targets naturally felled wood only. Other proxy-based reconstructions of sea ice, such as those derived from the IP_{25} biomarker, also suggest variability in sea ice cover during the Late Holocene associated with intermittent warm sea surface temperatures (Allaart et al., 2020; Jernas et al., 2013; Müller et al., 2012; Pawłowska et al., 2020; Sarnthein et al., 2003). Records of brine formation can be interpreted as a proxy for sea ice cover above basins, with a varied Late Holocene record from Storfjorden (Figure 1) suggesting episodic fluctuations between intense and reduced brine formation and concurrent sea ice cover variability (Rasmussen & Thomsen, 2014). A reconstruction of maximum sea ice extent in the Western Nordic Seas based upon tree ring chronologies and ice core oxygen isotopes (Macias-Fauria et al., 2010) again shows such variability, including the sea ice maxima during the LIA, and of record strong overall twentieth century decline.

4.1. Sources of Uncertainty

The utilization of the Weighed Score aids in reducing the bias of varied spatiotemporal coverage of the reference chronology, but sources of uncertainty do remain when interpreting the record. Late Holocene transgression may influence the preservation of older samples (Farnsworth, Allaart, et al., 2020; Forman et al., 2004). Degraded samples not included in the tree ring width data set (Figure 2) may have implications for observed Arctic driftwood densities, although these were predominantly observed at higher elevations than our target sampling sites at the modern day shoreline, suggesting older ages, and were often found from melting snowbanks and hence very moist. Given these more heavily degraded samples cannot be cross-referenced to our reference chronology, the ages of these ~30 samples are unknown. Therefore, when interpreting the contrasting regional trends in the earlier years of our data set (Figure 7), we assume that driftwood degradation is a risk equally applicable to all samples irrespective of their origin. Local sea ice conditions must also be considered when interpreting the driftwood record from these Svalbard collection sites, as persistent or semi-permanent land-fast ice resulting from localized cold conditions would minimize the transport of and catchment for driftwood accumulation (Funder et al., 2011), especially when considering that our sample sites are in the northernmost part of the archipelago.

Another feature to consider when utilizing and interpreting driftwood as a proxy for sea ice dynamics is the impact that circumpolar rivers flow regimes responsible for transporting driftwood from boreal forest zones to the Arctic basin may have played. Wohl et al. (2019) summarize these processes, whereby characteristics of flow are the first-order controls on wood transport, while spatial and temporal variation in channel and floodplain geometry, sediment inputs and mobility, wood piece size, and wood storage (e.g., dispersed pieces vs. jams) all influence wood transport. Variation in outflow and its impacts on sea ice also have an impact on driftwood transport (Park et al., 2020). Therefore, the survival and time delay between a boreal forest tree falling into a circumpolar river and entering the Arctic Ocean will be impacted by conditions affecting wood entrainment into channel margins and downstream transport such as channel size (Gregory et al., 2003), local flow regime and flow width and depth (Kramer & Wohl, 2017) and channel–floodplain connectivity (Wohl et al., 2018). Temporal factors such as spring melt, storms and flooding impacts these features and so also impacts downstream flow and ocean entry. Given the centennial spatiotemporal scope of the data set, and lack of sufficient available data on these variety of factors for the pan-Arctic across the past 500 years, these impacts are assumed not to have had a substantial impact on the trends observed.

5. Conclusions

We present a 500-year history of driftwood incursion to Northern Svalbard reflecting associated sea ice and Arctic Ocean circulation and provide for the first time a direct evaluation of sea ice dynamics inferred from naturally felled driftwood against the observational record. By crossdating samples against a circumpolar reference chronology across North American and Eurasian boreal forest zone drainage basins, a wide range of statistically significant matches can occur across the region, which would be considered a sign of good-fit by more restrictive references. To minimize the risk of bias toward regions covered by more reference chronologies, our study employs a novel approach to selecting probable origin sites, by weighting matches via reference chronology span and visualizing results through spatiotemporal density plots.

Our spatiotemporal record of driftwood incursion to northern Svalbard indicates centennial-to decadal-scale shifts in driftwood source regions, aligning with Late Holocene high variability and high frequency shifts in the TPD and BG strength and associated fluctuating climate conditions, and northward seasonal ice formation shift and migration of seasonal sea ice to the peripheral Arctic seas in the past century. In particular, we find that the increased spatio-temporal grain of the provenance of driftwood material informs not only about the relative contributions of the TPD and the BG (as in Funder et al., 2011), but also about the presence–or lack thereof–of sea ice in Arctic peripheral seas key to the global circulation (e.g., the Barents Sea), and of the overall sea ice conditions in the Arctic peripheral seas in general. A distinct decrease in driftwood incursion during the last 30 years matches the observed decline in pan-Arctic sea ice extent in recent decades, further highlighting the sensitivity of this unique sea ice proxy.

Overall, the inferred sea ice dynamics align well with other observations and proxy-based reconstruction across key points in the record (summarized in Table 1). With driftwood transport and deposition determined by sea ice and surface current dynamics, driftwood deposits on Arctic shorelines form a unique and currently under-utilized resource for the reconstruction of sea ice transport within large-scale Arctic Ocean circulations throughout the Holocene. Past driftwood dendrochronological studies have primarily been limited to geographically constrained settings or limited in the precision of provenance determination. This study is a step forward toward testing the validity of driftwood as a sea ice proxy, with driftwood-inferred sea ice conditions directly compared with the observational record for the first time. The study strengthens the use of dendro-provenancing as a method for increasing the spatiotemporal resolution of Arctic driftwood provenancing. Reconstructions of past sea ice conditions employing this proxy have scope for further development in the continued refinement of provenance and age determinations. With abundant driftwood deposits across the Arctic, this may enable a finer scale study of the role of atmospheric and oceanic circulation in sea ice and climatic changes throughout the Holocene.

Acknowledgments
G. M. Hole is funded by the Natural Environment Research Council (NERC grant: 1514291) and part of the Environmental Research Doctoral Training Program at the University of Oxford. Support and funding were also provided by M. Macias-Fauria and grant funds from NERC (NERC IRF grant: NE/L011859/1). T. Rawson is supported through an Engineering and Physical Sciences Research Council (EPSRC) (https://epsrc.ukri.org/) Systems Biology studentship award (EP/G03706X/1). Thanks to S. Brynjolfsson for assistance in sample collection during 2016 and 2018 at Wijdefjorden locations and to L. Allaart for leading funding of the 2018 field campaign to Vassfarbukta. The Wijdefjorden field campaigns in 2016 and 2018 were funded by grant numbers 16/35 (to W. R. Farnsworth) and 17/01132–3 (to LA) from the Svalbard Environmental Protection Fund respectively, Arctic Field grant no. 282643 awarded to LA by Svalbard Science Forum/Research Council of Norway, and the Arctic Research and Studies Program of the Ministries for Foreign Affairs of Norway and Iceland (grant agreement No. 2017-ARS-79772 to A. Schomacker). The authors also thank the anonymous reviewers for the helpful comments and suggestions received.

Data Availability Statement

All data used in this study are available at https://osf.io/z4t3a/.

References

Alkire, M. B., Morison, J., Schweiger, A., Zhang, J., Steele, M., Peralta-Ferriz, C., & Dickinson, S. (2017). A meteoric water budget for the Arctic Ocean. *Journal of Geophysical Research: Oceans*, *122*(12), 10020–10041. https://doi.org/10.1002/2017jc012807

Allaart, L., Müller, J., Schomacker, A., Rydningen, T. A., Håkansson, L., Kjellman, S. E., et al. (2020). Late quaternary glacier and sea-ice history of northern Wijdefjorden, Svalbard. *Boreas*, *49*(3), 417–437. https://doi.org/10.1111/bor.12435

Armand, L., Ferry, A., & Leventer, A. (2017). Advances in palaeo sea ice estimation. In *Sea ice* (pp. 600–629). Chichester: John Wiley & Sons Ltd.

Backman, J., Jakobsson, M., Løvlie, R., Polyak, L., & Febo, L. A. (2004). Is the central Arctic Ocean a sediment starved basin? *Quaternary Science Reviews*, *23*(11–13), 1435–1454. https://doi.org/10.1016/j.quascirev.2003.12.005

Baillie, M. G. L., & Pilcher, J. R. (1973). A simple crossdating program for tree-ring research. In *Tree ring Bulletin* (Vol. 33, pp. 7–14).

Barnes, E. A., & Screen, J. A. (2015). The impact of Arctic warming on the midlatitude jet-stream: Can it? Has it? Will it? *Wiley Interdisciplinary Reviews: Climate Change*, *6*(3), 277–286. https://doi.org/10.1002/wcc.337

Bartlein, P. J., Edwards, M. E., Hostetler, S. W., Shafer, S. L., Anderson, P. M., Brubaker, L. B., & Lozhkin, A. V. (2015). Early-Holocene warming in Beringia and its mediation by sea-level and vegetation changes. *Climate of the Past*, *11*(9), 1197–1222. https://doi.org/10.5194/cp-11-1197-2015

Belt, S. T. (2018). Source-specific biomarkers as proxies for Arctic and Antarctic sea ice. *Organic Geochemistry*, *125*, 277–298. https://doi.org/10.1016/j.orggeochem.2018.10.002

Belt, S. T., Massé, G., Rowland, S. J., Poulin, M., Michel, C., & LeBlanc, B. (2007). A novel chemical fossil of palaeo sea ice: IP25. *Organic Geochemistry*, *38*(1), 16–27. https://doi.org/10.1016/j.orggeochem.2006.09.013

Bengtsson, L., Semenov, V. A., & Johannessen, O. M. (2004). The early twentieth-century warming in the Arctic—A possible mechanism. *Journal of Climate*, *17*(20), 4045–4057. https://doi.org/10.1175/1520-0442(2004)017<4045:tetwit>2.0.co;2

Bigelow, N. H., Brubaker, L. B., Edwards, M. E., Harrison, S. P., Prentice, I. C., Anderson, P. M., et al. (2003). Climate change and Arctic ecosystems: 1. Vegetation changes north of 55°N between the last glacial maximum, mid-Holocene, and present. *Journal of Geophysical Research*, *108*(D19), 8170. https://doi.org/10.1029/2002jd002558

Bintanja, R., & Andry, O. (2017). Towards a rain-dominated Arctic. *Nature Climate Change*, *7*(4), 263–267. https://doi.org/10.1038/nclimate3240

Bjorkman, A. D., García Criado, M., Myers-Smith, I. H., Ravolainen, V., Jónsdóttir, I. S., Westergaard, K. B., et al. (2020). Status and trends in Arctic vegetation: Evidence from experimental warming and long-term monitoring. *Ambio*, *49*(3), 678–692. https://doi.org/10.1007/s13280-019-01161-6

Blake, W., Jr. (1961). In G. O. Raasch (ed.), *Radiocarbon dating of raised beaches in Nordaustlandet, Spitsbergen* (pp. 133, 146). University of Toronto Press. https://doi.org/10.3138/9781487584979-010

Bondevik, S., Mangerud, J., Ronnert, L., & Salvigsen, O. (1995). Postglacial sea-level history of Edgeøya and Barentsøya, eastern Svalbard. *Polar Research*, *14*(2), 153–180. https://doi.org/10.3402/polar.v14i2.6661

Carmack, E. C., Yamamoto-Kawai, M., Haine, T. W. N., Bacon, S., Bluhm, B. A., Lique, C., et al. (2016). Freshwater and its role in the Arctic marine system: Sources, disposition, storage, export, and physical and biogeochemical consequences in the Arctic and global oceans. *Journal of Geophysical Research: Biogeosciences*, *121*(3), 675–717. https://doi.org/10.1002/2015jg003140

Comiso, J. C., & Hall, D. K. (2014). Climate trends in the Arctic as observed from space. *Wiley Interdisciplinary Reviews: Climate Change*, *5*(3), 389–409. https://doi.org/10.1002/wcc.277

Cook, E. R., & Peters, K. (1997). Calculating unbiased tree-ring indices for the study of climatic and environmental change. *Holocene*, *7*(3), 361–370. https://doi.org/10.1177/095968369700700314

Cronin, T. M., Polyak, L., Reed, D., Kandiano, E. S., Marzen, R. E., & Council, E. A. (2013). A 600-ka Arctic sea-ice record from Mendeleev Ridge based on ostracodes. *Quaternary Science Reviews*, *79*, 157–167. https://doi.org/10.1016/j.quascirev.2012.12.010

Dalaiden, Q., Goosse, H., Lecomte, O., & Docquier, D. (2018). A model to interpret driftwood transport in the Arctic. *Quaternary Science Reviews*, *191*, 89–100. https://doi.org/10.1016/j.quascirev.2018.05.004

Daly, A. (2007). The Karschau ship, Schleswig-Holstein: Dendrochronological results and timber provenance. *International Journal of Nautical Archaeology*, *36*(1), 155–166. https://doi.org/10.1111/j.1095-9270.2006.00103.x

Daly, A., & Nymoen, P. (2008). The Bøle ship, Skien, Norway—Research history, dendrochronology and provenance. *International Journal of Nautical Archaeology*, *37*(1), 153–170. https://doi.org/10.1111/j.1095-9270.2007.00157.x

De Vernal, A., Hillaire-Marcel, C., Rochon, A., Fréchette, B., Henry, M., Solignac, S., & Bonnet, S. (2013). Dinocyst-based reconstructions of sea ice cover concentration during the Holocene in the Arctic Ocean, the northern North Atlantic Ocean and its adjacent seas. *Quaternary Science Reviews*, *79*, 111–121. https://doi.org/10.1016/j.quascirev.2013.07.006

Dieckmann, G. S., & Hellmer, H. H. (2010). The importance of sea ice: An overview. *Sea Ice*, *2*, 1–22.

Ding, Q., Schweiger, A., Battisti, D. S., Johnson, N. C., Wrigglesworth, E. B., Zhang, Q., et al. (2017). Influence of the recent high-latitude atmospheric circulation change on summertime Arctic sea ice. *March*, *7*, 289–295. https://doi.org/10.1038/NCLIMATE3241

Divine, D. V., & Dick, C. (2006). Historical variability of sea ice edge position in the Nordic Seas. *Journal of Geophysical Research*, *111*(C1), C01001. https://doi.org/10.1029/2004jc002851

Drake, B. L. (2018). Source & Sourceability: Towards a probabilistic framework for dendroprovenance based on hypothesis testing and Bayesian inference. *Dendrochronologia*, *47*, 38–47. https://doi.org/10.1016/j.dendro.2017.12.004

Dyke, A. S., England, J. H., Reimnitz, E., & Jetté, H. (1997). Changes in driftwood delivery to the Canadian Arctic Archipelago: The hypothesis of postglacial oscillations of the transpolar drift. *Arctic*, *50*(1), 1–16. https://doi.org/10.14430/arctic1086

Dyke, A. S., & Savelle, J. M. (2000). Holocene driftwood incursion to southwestern Victoria Island, Canadian Arctic Archipelago, and its significance to paleoceanography and archaeology. *Quaternary Research*, *54*(1), 113–120. https://doi.org/10.1006/qres.2000.2141

Eckstein, D., & Bauch, J. (1969). Beitrag zur Rationalisierung eines dendrochronologischen Verfahrens und zur Analyse seiner Aussagesicherheit. *Forstwissenschaftliches Centralblatt*, *88*(1), 230–250. https://doi.org/10.1007/BF02741777

Eggertsson, Ó. (1993). Origin of the driftwood on the coasts of Iceland; a dendrochronological study. *Jökull*, *43*, 15–32.

Eggertsson, Ó., & Laeyendecker, D. (1995). A dendrochronological study of the origin of driftwood in Frobisher Bay, Baffin Island, NWT, Canada. *Arctic and Alpine Research*, *27*(2), 180–186. https://doi.org/10.2307/1551900

Fagel, N., Not, C., Gueibe, J., Mattielli, N., & Bazhenova, E. (2014). Late Quaternary evolution of sediment provenances in the Central Arctic Ocean: Mineral assemblage, trace element composition and Nd and Pb isotope fingerprints of detrital fraction from the Northern Mendeleev Ridge. *Quaternary Science Reviews*, *92*, 140–154. https://doi.org/10.1016/j.quascirev.2013.12.011

Farnsworth, W. R., Allaart, L., Ingólfsson, Ó., Alexanderson, H., Forwick, M., Noormets, R., et al. (2020). Holocene glacial history of Svalbard: Status, perspectives and challenges. *Earth-Science Reviews*, *208*, 103249. https://doi.org/10.1016/j.earscirev.2020.103249

Farnsworth, W. R., Blake, W., Jr., Guðmundsdóttir, E. R., Ingólfsson, Ó., Kalliokoski, M. H., Larsen, G., et al. (2020). Ocean-rafted pumice constrains postglacial relative sea-level and supports Holocene ice cap survival. *Quaternary Science Reviews*, *250*, 106654. https://doi.org/10.1016/j.quascirev.2020.106654

Feyling-Hanssen, R. W., & Olsson, I. (1959). Five radiocarbon datings of post glacial shorelines in central Spitsbergen. *Norsk Geografisk Tidsskrift — Norwegian Journal of Geography*, *17*(1–4), 122–131. https://doi.org/10.1080/00291955908551761

Forman, S. L. (1990). Post-glacial relative sea-level history of northwestern Spitsbergen, Svalbard. *Geological Society of America Bulletin*, *102*(11), 1580–1590. https://doi.org/10.1130/0016-7606(1990)102<1580:pgrslh>2.3.co;2

Forman, S. L., & Ingólfsson, Ó. (2000). Late Weichselian glacial history and postglacial emergence of Phippsøya, Sjuøyane, northern Svalbard: A comparison of modelled and empirical estimates of a glacial-rebound hinge line. *Boreas*, *29*(1), 16–25. https://doi.org/10.1111/j.1502-3885.2000.tb01197.x

Forman, S. L., Lubinski, D. J., Ingólfsson, Ó., Zeeberg, J. J., Snyder, J. A., Siegert, M. J., & Matishov, G. G. (2004). A review of postglacial emergence on Svalbard, Franz Josef Land and Novaya Zemlya, northern Eurasia. *Quaternary Science Reviews*, *23*(11–13), 1391–1434. https://doi.org/10.1016/j.quascirev.2003.12.007

Francis, J. A., & Vavrus, S. J. (2012). Evidence linking Arctic amplification to extreme weather in mid-latitudes. *Geophysical Research Letters*, *39*, L06801. https://doi.org/10.1029/2012GL051000

Funder, S., Goosse, H., Jepsen, H., Kaas, E., Kjær, K. H., Korsgaard, N. J., et al. (2011). A 10,000-year record of Arctic ocean sea-ice variability-view from the beach. *Science*, *333*(6043), 747–750. https://doi.org/10.1126/science.1202760

Gossett, J. (1996). Arctic research using nuclear submarines. *Oceanographic Literature Review*, *43*(11), 1171.
Gregory, S., Boyer, K. L., & Gurnell, A. M. (2003). *Ecology and management of wood in world rivers.* Corvallis, Or: International conference of wood in World rivers.
Grissino-Mayer, H. D., & Fritts, H. C. (1997). The international tree-ring data bank: An enhanced global database serving the global scientific community. *The Holocene*, *7*(2), 235–238. https://doi.org/10.1177/095968369700700212
Haas, C., & Thomas, D. N. (2017). Sea ice thickness distribution. In *Sea ice* (pp. 42–64). Wiley.
Häggblom, A., & Haggblom, A. (1982). Driftwood in Svalbard as an indicator of sea ice conditions. *Geografiska Annaler — Series A: Physical Geography*, *64*(1/2), 81–94. https://doi.org/10.2307/520496
Hellmann, L., Agafonov, L., Ljungqvist, F. C., Churakova, O., Düthorn, E., Esper, J., et al. (2016). Diverse growth trends and climate responses across Eurasia's boreal forest. *Environmental Research Letters*, *11*(7), 74021. https://doi.org/10.1088/1748-9326/11/7/074021
Hellmann, L., Tegel, W., Eggertsson, Ó., Schweingruber, F. H., Blanchette, R. A., Kirdyanov, A., et al. (2013). Tracing the origin of Arctic driftwood. *Journal of Geophysical Research: Biogeosciences*, *118*(1), 68–76. https://doi.org/10.1002/jgrg.20022
Hellmann, L., Tegel, W., Geyer, J., Kirdyanov, A. V., Nikolaev, A. N., Eggertsson, Ó., et al. (2017). Dendro-provenancing of Arctic driftwood. *Quaternary Science Reviews*, *162*, 1–11. https://doi.org/10.1016/j.quascirev.2017.02.025
Hillaire-Marcel, C., Maccali, J., Not, C., & Poirier, A. (2013). Geochemical and isotopic tracers of Arctic sea ice sources and export with special attention to the Younger Dryas interval. *Quaternary Science Reviews*, *79*, 184–190. https://doi.org/10.1016/j.quascirev.2013.05.001
Hole, G. M., & Macias-Fauria, M. (2017). Out of the woods: Driftwood insights into Holocene pan-Arctic sea ice dynamics. *Journal of Geophysical Research: Oceans*, *122*(9), 7612–7629. https://doi.org/10.1002/2017JC013126
Holmes, R. L. (1983). *Computer-assisted quality control in tree-ring dating and measurement*.
Hopkins, D. M., Smith, P. A., & Matthews, J. V. (1981). Dated wood from Alaska and the Yukon: Implications for forest refugia in Beringia. *Quaternary Research*, *15*(3), 217–249. https://doi.org/10.1016/0033-5894(81)90028-4
Hughes, M. K., Milsom, S. J., & Leggett, P. A. (1981). Sapwood estimates in the interpretation of tree-ring dates. *Journal of Archaeological Science*, *8*(4), 381–390. https://doi.org/10.1016/0305-4403(81)90037-6
Ingólfsson, Ó., & Landvik, J. Y. (2013). The Svalbard–Barents sea ice-sheet – Historical, current and future perspectives. *Quaternary Science Reviews*, *64*, 33–60. https://doi.org/10.1016/j.quascirev.2012.11.034
Jernas, P., Klitgaard Kristensen, D., Husum, K., Wilson, L., & Koç, N. (2013). Palaeoenvironmental changes of the last two millennia on the western and northern Svalbard shelf. *Boreas*, *42*(1), 236–255. https://doi.org/10.1111/j.1502-3885.2012.00293.x
Kinnard, C., Zdanowicz, C. M., Fisher, D. A., Isaksson, E., de Vernal, A., & Thompson, L. G. (2011). Reconstructed changes in Arctic sea ice over the past 1,450 years. *Nature*, *479*(7374), 509–512. https://doi.org/10.1038/nature10581
Kinnard, C., Zdanowicz, C. M., Koerner, R. M., & Fisher, D. A. (2008). A changing Arctic seasonal ice zone: Observations from 1870–2003 and possible oceanographic consequences. *Geophysical Research Letters*, *35*(2), L02507. https://doi.org/10.1029/2007gl032507
Koch, J. (2009). Improving age estimates for late Holocene glacial landforms using dendrochronology–Some examples from Garibaldi Provincial Park, British Columbia. *Quaternary Geochronology*, *4*(2), 130–139. https://doi.org/10.1016/j.quageo.2008.11.002
Kramer, N., & Wohl, E. (2017). Rules of the road: A qualitative and quantitative synthesis of large wood transport through drainage networks. *Geomorphology*, *279*, 74–97. https://doi.org/10.1016/j.geomorph.2016.08.026
Kwok, R., Spreen, G., & Pang, S. (2013). Arctic sea ice circulation and drift speed: Decadal trends and ocean currents. *Journal of Geophysical Research: Oceans*, *118*(5), 2408–2425. https://doi.org/10.1002/jgrc.20191
Linderholm, H. W., Gunnarson, B. E., Fuentes, M., Büntgen, U., & Hormes, A. (2021). The origin of driftwood on eastern and south-western Svalbard. *Polar Science*, 100658. https://doi.org/10.1016/j.polar.2021.100658
MacDonald, G. M., Kremenetski, K. V., & Beilman, D. W. (2008). Climate change and the northern Russian treeline zone. *Philosophical Transactions of the Royal Society of London. Series B, Biological Sciences*, *363*(1501), 2285–2299. https://doi.org/10.1098/rstb.2007.2200
MacDonald, G. M., Velichko, A. A., Kremenetski, C. V., Borisova, O. K., Goleva, A. A., Andreev, A. A., et al. (2000). Holocene treeline history and climate change across northern Eurasia. *Quaternary Research*, *53*(3), 302–311. https://doi.org/10.1006/qres.1999.2123
Macias-Fauria, M., Grinsted, A., Helama, S., Moore, J., Timonen, M., Martma, T., et al. (2010). Unprecedented low twentieth century winter sea ice extent in the Western Nordic Seas since A.D. 1200. *Climate Dynamics*, *34*(6), 781–795. https://doi.org/10.1007/s00382-009-0610-z
Macias-Fauria, M., & Post, E. (2018). Effects of sea ice on Arctic biota: An emerging crisis discipline. *Biology Letters*, *14*(3), 20170702. https://doi.org/10.1098/rsbl.2017.0702
Mahoney, A. R., Hutchings, J. K., Eicken, H., & Haas, C. (2019). Changes in the thickness and circulation of multiyear ice in the Beaufort Gyre determined from pseudo-Lagrangian methods from 2003–2015. *Journal of Geophysical Research: Oceans*, *124*(8), 5618–5633. https://doi.org/10.1029/2018jc014911
Maslowski, W., Clement Kinney, J., Higgins, M., & Roberts, A. (2012). The future of Arctic sea ice. *Annual Review of Earth and Planetary Sciences*, *40*(1), 625–654. https://doi.org/10.1146/annurev-earth-042711-105345
McLaren, A. S. (1989). The under-ice thickness distribution of the Arctic Basin as recorded in 1958 and 1970. *Journal of Geophysical Research*, *94*(C4), 4971–4983. https://doi.org/10.1029/JC094iC04p04971
Mette, M. J., Wanamaker, A. D., Jr., Retelle, M. J., Carroll, M. L., Andersson, C., & Ambrose, W. G., Jr. (2021). Persistent multidecadal variability since the 15th century in the southern Barents Sea derived from annually resolved shell-based records. *Journal of Geophysical Research: Oceans*, *126*, e2020JC017074. https://doi.org/10.1029/2020jc017074
Mörner, N.-A., Solheim, J.-E., Humlum, O., & Falk-Petersen, S. (2020). Changes in Barents Sea ice edge positions in the last 440 years: A review of possible driving forces. *International Journal of Astronomy and Astrophysics*, *10*(02), 97.
Müller, J., Wagner, A., Fahl, K., Stein, R., Prange, M., & Lohmann, G. (2011). Towards quantitative sea ice reconstructions in the northern North Atlantic: A combined biomarker and numerical modelling approach. *Earth and Planetary Science Letters*, *306*(3–4), 137–148. https://doi.org/10.1016/j.epsl.2011.04.011
Müller, J., Werner, K., Stein, R., Fahl, K., Moros, M., & Jansen, E. (2012). Holocene cooling culminates in sea ice oscillations in Fram Strait. *Quaternary Science Reviews*, *47*, 1–14. https://doi.org/10.1016/j.quascirev.2012.04.024
Nixon, F. C., England, J. H., Lajeunesse, P., & Hanson, M. A. (2016). An 11 000-year record of driftwood delivery to the western Queen Elizabeth Islands, Arctic Canada. *Boreas*, *45*(3), 494–507. https://doi.org/10.1111/bor.12165
Norwegian Polar Institute. (2014). *Kartdata svalbard 1:100 000 (S100 Kartdata)/Map data* [data set]. Norwegian Polar Institute. https://doi.org/10.21334/npolar.2014.645336c7
Ogilvie, A. E. J., & Jónsdóttir, I. (2000). Sea ice, climate, and Icelandic fisheries in the eighteenth and nineteenth centuries. *Arctic*, *53*(4), 383–394. https://doi.org/10.14430/arctic869
Overland, J. E., Dethloff, K., Francis, J. A., Hall, R. J., Hanna, E., Kim, S.-J., et al. (2016). Nonlinear response of mid-latitude weather to the changing Arctic. *Nature Climate Change*, *6*(11), 992–999. https://doi.org/10.1038/nclimate3121

Overland, J. E., & Wang, M. (2010). Large-scale atmospheric circulation changes are associated with the recent loss of Arctic sea ice. *Tellus, Series A: Dynamic Meteorology and Oceanography*, *62*(1), 1–9. https://doi.org/10.1111/j.1600-0870.2009.00421.x

Owczarek, P. (2010). Dendrochronological dating of geomorphic processes in the High Arctic. *Landform Analysis*, *14*, 45–56.

Panteleev, G., Proshutinsky, A., Kulakov, M., Nechaev, D. A., & Maslowski, W. (2007). Investigation of the summer Kara Sea circulation employing a variational data assimilation technique. *Journal of Geophysical Research*, *112*(C4), C04S15. https://doi.org/10.1029/2006jc003728

Park, H., Watanabe, E., Kim, Y., Polyakov, I., Oshima, K., Zhang, X., et al. (2020). Increasing riverine heat influx triggers Arctic sea ice decline and oceanic and atmospheric warming. *Science Advances*, *6*(45), eabc4699. https://doi.org/10.1126/sciadv.abc4699

Pavlov, V. K., & Pfirman, S. L. (1995). Hydrographic structure and variability of the Kara Sea: Implications for pollutant distribution. *Deep-Sea Research Part II*, *42*(6), 1369–1390. https://doi.org/10.1016/0967-0645(95)00046-1

Pawłowska, J., Łącka, M., Kucharska, M., Pawlowski, J., & Zajączkowski, M. (2020). Multiproxy evidence of the Neoglacial expansion of Atlantic water to eastern Svalbard. *Climate of the Past*, *16*(2), 487–501. https://doi.org/10.5194/cp-16-487-2020

Polyak, L., Alley, R. B., Andrews, J. T., Brigham-Grette, J., Cronin, T. M., Darby, D. A., et al. (2010). History of sea ice in the Arctic. *Quaternary Science Reviews*, *29*(15–16), 1757–1778. https://doi.org/10.1016/j.quascirev.2010.02.010

Post, E., & Høye, T. T. (2013). Advancing the long view of ecological change in tundra systems. *Philosophical Transactions of the Royal Society of London B Biological Sciences*, *368*(1624). https://doi.org/10.1098/rstb.2012.0477

Rasmussen, T. L., & Thomsen, E. (2014). Brine formation in relation to climate changes and ice retreat during the last 15,000 years in Storfjorden, Svalbard, 76–78°N. *Paleoceanography*, *29*(10), 911–929. https://doi.org/10.1002/2014pa002643

Rigor, I. G., Wallace, J. M., & Colony, R. L. (2002). Response of sea ice to the Arctic oscillation. *Journal of Climate*, *15*(18), 2648–2663. https://doi.org/10.1175/1520-0442(2002)015<2648:ROSITT>2.0.CO;2

Rinn, F. (2003). *TSAP-Win. Time series analysis and presentation for dendrochronology and 409 related applications. User Reference.*

Ritchie, J. C., & Hare, F. K. (1971). Late-quaternary vegetation and climate near the arctic tree line of northwestern North America. *Quaternary Research*, *1*(3), 331–342. https://doi.org/10.1016/0033-5894(71)90069-X

Rothrock, D. A., Percival, D. B., & Wensnahan, M. (2008). The decline in arctic sea-ice thickness: Separating the spatial, annual, and interannual variability in a quarter century of submarine data. *Journal of Geophysical Research*, *113*(5), 1–9. https://doi.org/10.1029/2007JC004252

Sander, L., Kirdyanov, A., Crivellaro, A., & Büntgen, U. (2021). Short communication: Driftwood provides reliable chronological markers in Arctic coastal deposits. *Geochronology*, *3*(1), 171–180. https://doi.org/10.5194/gchron-3-171-2021

Sarnthein, M., Van Kreveld, S., Erlenkeuser, H., Grootes, P. M., Kucera, M., Pflaumann, U., & Schulz, M. (2003). Centennial-to-millennial-scale periodicities of Holocene climate and sediment injections off the western Barents shelf, 75 N. *Boreas*, *32*(3), 447–461. https://doi.org/10.1080/03009480301813

Schomacker, A., Farnsworth, W. R., Ingólfsson, Ó., Allaart, L., Håkansson, L., Retelle, M., et al. (2019). Postglacial relative sea level change and glacier activity in the early and late Holocene: Wahlenbergfjorden, Nordaustlandet, Svalbard. *Scientific Reports*, *9*(1), 6799. https://doi.org/10.1038/s41598-019-43342-z

Schweingruber, F. H. (2012). *Tree rings: Basics and applications of dendrochronology*. Springer Science and Business Media.

Schytt, V., Hoppe, G., Blake, W., Jr., & Grosswald, M. G. (1968). The extent of the Würm glaciation in the European Arctic. *International Association of Hydrological Sciences*, *79*, 207–216.

Screen, J. A., & Simmonds, I. (2010). The central role of diminishing sea ice in recent Arctic temperature amplification. *Nature*, *464*(7293), 1334–1337. https://doi.org/10.1038/nature09051

Screen, J. A., & Simmonds, I. (2014). Amplified mid-latitude planetary waves favour particular regional weather extremes. *Nature Climate Change*, *4*, 704–709. https://doi.org/10.1038/NCLIMATE2271

Seidenkrantz, M. S. (2013). Benthic foraminifera as palaeo sea-ice indicators in the subarctic realm — Examples from the Labrador Sea-Baffin Bay region. *Quaternary Science Reviews*, *79*, 135–144. https://doi.org/10.1016/j.quascirev.2013.03.014

Serreze, M. C., Barrett, A. P., Slater, A. G., Woodgate, R. A., Aagaard, K., Lammers, R. B., et al. (2006). The large-scale freshwater cycle of the Arctic. *Journal of Geophysical Research*, *111*(11), 1–19. https://doi.org/10.1029/2005JC003424

Serreze, M. C., & Francis, J. A. (2006). The Arctic amplification debate. *Climatic Change*, *76*(3), 241–264. https://doi.org/10.1007/s10584-005-9017-y

Shapiro, I., Colony, R., & Vinje, T. (2003). April sea ice extent in the Barents Sea, 1850 – 2001. *Polar Research*, *22*(1), 5–10. https://doi.org/10.1111/j.1751-8369.2003.tb00089.x

Smedsrud, L. H., Esau, I., Ingvaldsen, R. B., Eldevik, T., Haugan, P. M., Li, C., et al. (2013). The role of the Barents Sea in the Arctic climate system. *Reviews of Geophysics*, *51*(3), 415–449. https://doi.org/10.1002/rog.20017

Sokolov, S. Y., Svyazeva, O. A., & Kubli, V. A. (1977). *Arealy Derev Ev I Kustarnikov SSSR [Ranges of Trees and Shrubs of the USSR* (Vol. 1). Leningrad: Nauka.

Stickley, C. E., St John, K., Koç, N., Jordan, R. W., Passchier, S., Pearce, R. B., & Kearns, L. E. (2009). Evidence for middle Eocene Arctic sea ice from diatoms and ice-rafted debris. *Nature*, *460*(7253), 376–379. https://doi.org/10.1038/nature08163

Taylor, R. E., & Aitken, M. J. (1997). *Chronometric dating in archaeology* (Vol. 2). Springer Science and Business Media.

Thompson, D. W. J., & Wallace, J. M. (1998). The Arctic oscillation signature in the wintertime geopotential height and temperature fields. *Geophysical Research Letters*, *25*(9), 1297–1300. https://doi.org/10.1029/98GL00950

Timmermans, M.-L., Toole, J., & Krishfield, R. (2018). Warming of the interior Arctic Ocean linked to sea ice losses at the basin margins. *Science Advances*, *4*(8), eaat6773. https://doi.org/10.1126/sciadv.aat6773

Tremblay, L.-B., Mysak, L. A., & Dyke, A. S. (1997). Evidence from driftwood records for century-to-millennial scale variations of the high latitude atmospheric circulation during the Holocene. *Geophysical Research Letters*, *24*(16), 2027–2030. https://doi.org/10.1029/97GL02028

Vare, L. L., Massé, G., & Belt, S. T. (2010). A biomarker-based reconstruction of sea ice conditions for the Barents Sea in recent centuries. *The Holocene*, *20*(4), 637–643. https://doi.org/10.1177/0959683609355179

Vavrus, S. J., Wang, F., Martin, J. E., Francis, J. A., Peings, Y., & Cattiaux, J. (2017). Changes in North American atmospheric circulation and extreme weather: Influence of Arctic amplification and northern hemisphere snow cover. *Journal of Climate*, *30*, 4317–4333. https://doi.org/10.1175/JCLI-D-16-0762.1

Vinje, T. (2001). Anomalies and trends of sea-ice extent and atmospheric circulation in the Nordic Seas during the period 1864–1998. *Journal of Climate*, *14*(3), 255–267. https://doi.org/10.1175/1520-0442(2001)014<0255:AATOSI>2.0.CO;2

Voronina, E., Polyak, L., Vernal, A. D., & Peyron, O. (2001). Holocene variations of sea-surface conditions in the southeastern Barents Sea, reconstructed from dinoflagellate cyst assemblages. *Journal of Quaternary Science: Published for the Quaternary Research Association*, *16*(7), 717–726. https://doi.org/10.1002/jqs.650

Walsh, J. E., Fetterer, F., Scott Stewart, J., & Chapman, W. L. (2017). A database for depicting Arctic sea ice variations back to 1850. *Geographical Review*, *107*(1), 89–107. https://doi.org/10.1111/j.1931-0846.2016.12195.x

Wilson, L. J., Hald, M., & Godtliebsen, F. (2011). Foraminiferal faunal evidence of twentieth-century Barents sea warming. *The Holocene*, *21*(4), 527–537. https://doi.org/10.1177/0959683610385718

Wohl, E., Cadol, D., Pfeiffer, A., Jackson, K., & Laurel, D. (2018). Distribution of large wood within river corridors in relation to flow regime in the semiarid western US. *Water Resources Research*, *54*(3), 1890–1904. https://doi.org/10.1002/2017wr022009

Wohl, E., Kramer, N., Ruiz-Villanueva, V., Scott, D. N., Comiti, F., Gurnell, A. M., et al. (2019). The natural wood regime in rivers. *BioScience*, *69*(4), 259–273. https://doi.org/10.1093/biosci/biz013

Woodgate, R. A. (2018). Increases in the Pacific inflow to the Arctic from 1990 to 2015, and insights into seasonal trends and driving mechanisms from year-round Bering Strait mooring data. *Progress in Oceanography*, *160*, 124–154. https://doi.org/10.1016/j.pocean.2017.12.007

Zeeberg, J., Lubinski, D. J., & Forman, S. L. (2001). Holocene relative sea-level history of Novaya Zemlya, Russia, and implications for Late Weichselian ice-sheet loading. *Quaternary Research*, *56*(2), 218–230. https://doi.org/10.1006/qres.2001.2256

Zhang, Q., Xiao, C., Ding, M., & Dou, T. (2018). Reconstruction of autumn sea ice extent changes since AD1289 in the Barents-Kara Sea, Arctic. *Science China Earth Sciences*, *61*(9), 1279–1291.